Check for updates

Structure properties and industrial applications of anion exchange resins for the removal of electroactive nitrate ions from contaminated water

Mohammad Faraz Ahmer[a] and Mohammad Kashif Uddin ✪ *[b]

The presence of nitrates in lakes, rivers, and groundwater is common. Anion exchange resins (AER) are polymeric structures that contain functional groups as well as a variety of particle sizes that are used for removing nitrate ions from solutions. This article provides a concise review of the types and properties of AER, synthesis methods, characterization, and environmental applications of AER. It discusses how different factors affect the adsorption process, isotherm and kinetic parameters, the adsorption mechanism, and the maximum adsorption capacities. Additionally, the present review addresses AER's regeneration and practical stability. It emphasizes the progress and proposes future strategies for addressing nitrate pollution using AER to overcome the challenges. This review aims to act as a reference for researchers working in the advancement of ion exchange resins and presents a clear and concise scientific analysis of the use of AER in nitrate adsorption. It is evident from the literature survey that AER is highly effective at removing nitrate ions from wastewater effluents.

[a]*Department of Electrical and Electronics Engineering, Mewat Engineering College, Gurugram University, Nuh 122107, Haryana, India. E-mail: farazahmer007@gmail.com*

[b]*Department of Chemistry, College of Science, Majmaah University, Al-Zulfi Campus, Al-Majmaah 11952, Kingdom of Saudi Arabia. E-mail: mohdkashifchem@gmail.com; m.kashifuddin@mu.edu.sa*

1. Introduction

In many countries around the world, increasing population has put a focus on ensuring affordable water supply and sustainable management of water resources to limit the shortage of drinking water. Unlike surface water, groundwater contains a higher concentration of abundant dissolved constituents such as cations and anions. The chemical quality of water can be ascertained by measuring the concentration level of constituent

*Dr Mohammad Faraz Ahmer is working as Assistant Professor in the Department of Electrical and Electronics Engineering, Nuh, Gurugram University since 2012. He completed his B. E. and M. Tech. degrees from A.M.U., Aligarh and Ph.D. from Shri Venkateshwara University, Gajraula. He has published **30** research papers/book chapters and attended/presented research papers in several National/International confer-*

Mohammad Faraz Ahmer

*ences. In collaboration, with others he has edited **10** books. He is co-supervisor of **one** Ph.D. student working at J.M.I. New Delhi. His areas of research interest are AGC, Renewable Energy Sources and Green Analytical/Energy techniques.*

Dr Mohammad Kashif Uddin received his M.Phil. (2008) and Ph.D. (2012) in Applied Chemistry from Aligarh Muslim University, India. His academic career started at the Majmaah University, Saudi Arabia in 2013. Here in 2022, he was promoted to Associate Professor. He teaches various chemistry courses. His research focuses on water treatment and environmental nanotechnology. He has published 39 publications in

Mohammad Kashif Uddin

this field, including research and review articles, book chapters, and conference papers. He has received several research awards.

charged species, *i.e.* cations and anions. Several international public health organizations have set standards for ionic concentrations in groundwater that have been accepted by governments to assess drinking water quality. Table 1 presents the World Health Organization's (WHO) drinking-water quality standards for anion concentrations.[1] Several body functions require electrolytes, which are present in cells and fluids of the body, so consuming them from food is essential. A change in the concentration of dissolved ions causes saline toxicity in water when it turns out to be away from the set standards. Therefore, it is important to identify increased ion concentrations in water since they may affect the health of humans and aquatic organisms. Increased levels of several ions cause water hardness, and the high salt concentration in water systems leads to chronic toxicity to algae and aquatic plants.[2] Normally, cations and anions are mingled with other ions, so it is also necessary to measure the toxicity of combined ions in water as insoluble compounds.

To address the challenge of industrial discharged wastewater, various water treatment processes, including conventional processes, have been developed over the years such as boiling,[3] flocculation,[4] coagulation,[5] filtration,[6] chlorination,[7] and comparably advanced processes such as adsorption,[8,9] reverse osmosis,[10] membrane filtration,[11] and advanced oxidation[12] such as photocatalysis[13] and photo-Fenton.[14,15] Ion exchange processes play a significant role in separating, purifying, and decontaminating ions-containing solutions. Ion exchange is exceptionally efficient at extracting certain ions from water, which makes it especially suitable for processes like water softening and deionization. The method is efficient and facilitates the simple extraction of metals from wastewater. Ion exchange offers benefits over alternative purification methods, such as lower operational costs, and the capability of high purity through targeted ion removal. It also offers ease of handling, minimal chemical usage, and the ability to recover substances through resin regeneration. Moreover, ion exchange systems can be regenerated and recycled, enhancing their economic viability and environmental sustainability. Ion exchange processes continue to be researched by scientists to introduce advanced properties, cost-effectiveness, and new applications. Ion exchange resin is a cross-linked, insoluble

polymer that represents the major class of ion exchange processes and acts as a carrier for the stoichiometric exchange of ions. Since ion exchange resins have acidic or basic functional groups in their molecular structure, they are broadly divided into two groups: cation exchange resin and anion exchange resin. In cation exchange resins, the functional groups are acidic, such as sulfonic ($-SO_3H$), carboxyl ($-COOH$), phosphate ($-PO_4^{3-}$), *etc.* In anion exchange resins, the functional groups are basic, such as quaternary ammonium groups ($-NH_4^+$), amino ($-NH_2$), phosphine ($-PR_3^+$), *etc.* Cation-exchange resins contain negative charge (anions) on the polymer backbone and thus attract positive ions (cations). Anion exchange materials instead contain a positive charge on the backbone of the material, attracting anions. The ion exchange resin is generally formed by the polymerization process where one or more chemical treatments are applied to produce various functional groups. Ion exchange resins are used as stationary phases in ion-exchange chromatography. A notable use of ion exchange resins is their ability to remove chemical contaminants from aqueous solutions. Several reviews have been published targeting the removal of various types of pollutants *via* ion-exchange sorbents,[16] including boron,[17] organic matter,[18] reactive dyes,[19] and poly-fluoroalkyl substances.[20] This review paper specifically focuses on anion exchange resins, and hence, the literature was specifically gathered regarding the properties and applications of anion exchange resins in nitrate adsorption. It is an important review highlighting the effectiveness of anion exchange resins in removing nitrate ions from contaminated water. The goal of this paper is not only to provide background information from existing literature but also to offer an up-to-date review of this new topic to aid researchers in designing future studies.

2. Nitrate ions, their sources, toxicity, and removal techniques

The existence of nitrogen is essential for the survival of all living organisms. Nitrogen is crucial for crops. It can be applied to soil through organic means such as manure, or synthetic fertilizers like urea and ammonia.[21] Nitrogen compounds, including ammonia, nitrite, and nitrate play a crucial role in our environment. Plants need nitrogen to grow, but its overabundance from human activities can adversely affect water quality. The maintenance of a healthy aquatic environment depends on proper management and awareness. In groundwater, nitrogen, known as nitrate, can contaminate drinking water by leaching into the ground or runoff into surface water. When groundwater containing nitrates flows into water bodies, it can lead to a process called "Eutrophication". This process occurs when a body of water becomes overloaded with excessive nutrients, thereby causing an overgrowth of plants and algae. Such overgrowth can decrease oxygen levels in water. This can detriment aquatic organisms, disrupt ecosystem balance, and even collapse entire aquatic ecosystems. The recommended nitrate level in drinking water should not exceed 10 mg L^{-1}.[22] The high solubility of nitrate in water and the difficulty of fixing it in the soil make it the

Table 1 WHO guidelines for drinking-water quality[1]

Ions	Permissible limit (mg L^{-1})
Boron compounds	2.4
Bromate	0.4
Bromide	NA
Chloride	NA
Chlorine	5
Fluoride	1.5
Iodine	NA
Nitrate	50
Nitrite	3
Perchlorate	0.07
Sulfate	NA

most prevalent pollutant in groundwater.[23] Most nitrates humans consume come from vegetables and drinking water sources.[24] Exposure to nitrates and nitrites can have adverse health effects, such as methemoglobinemia.[25] In severe cases, it can lead to attacks, a coma, and even death.[26] A variety of plant-related nitrate/nitrite poisonings in cattle, goats, pigs, and sheep have been reported from many different places in the world.[27] There is evidence that certain aquatic animals may be at risk due to nitrate discharges from human sources.[28] The cause of the sudden death of ducks at Mettukolathur farm, Kancheepuram district, India was nitrate poisoning.[29] There are serious health risks associated with drinking water containing high levels of nitrate to humans, especially to infants and pregnant women. The WHO sets the nitrate limit at 50 mg L^{-1} for adults and 15 mg L^{-1} for children.[30] Excessive nitrates may cause eutrophication in aquatic systems, leading to oxygen-depleting algal blooms that endanger marine life. Consequently, nitrate pollution in both groundwater and surface water is a significant and hazardous problem. This makes nitrate removal a critical task. According to a recent review article,[31] the presence of nitrate and nitrite in drinking water increases cancer risk. It is therefore vital to thoroughly explore the issue of groundwater pollution and, in particular, the presence of nitrates.[32] It is essential to monitor nitrate levels in water sources regularly to ensure they stay within safe parameters. Frequent testing can identify pollution promptly, facilitating intervention and remediation. Such preventative measures safeguard public health and guarantee clean drinking water for communities. It is vital to eliminate nitrate ions from the water before human consumption, achievable through many water filtration techniques. Moreover, since excessive boiling can increase nitrate concentration, it is advisable to boil water only until it reaches a rolling boil to maintain microbiological safety.

It is a growing concern worldwide that groundwater nitrate content is increasing. A total of 292 points from 146 published works analyzed in a literature review were used to compare the nitrate concentration of different groundwater bodies worldwide.[32] The primary cause of NO$_3^-$ pollution is agriculture, specifically, fertilizers and pesticides. Asia and Africa reported the significant presence of NO$_3^-$ because of the heavy rainfall and the pitiable management of sewage-disposal. In America, aquifers are impacted by wastewater discharges without appropriate treatment. In Europe, waste disposal, industrial activities, and sewage contribute to the nitrate presence in groundwater. A recent study[33] reviewed 94 scholarly articles on NO$_3^-$ pollution to investigate the geospatial distribution of nitrate concentrations in the Indo-Gangetic Plain, and their possible sources and related health risks.

Nitrate (NO$_3^-$) can be removed from drinking water using a variety of methods and industrial technologies, including biological and physicochemical methods.[34–36] It has been reported in many reviews that nitrate adsorption is effective.[23,37–41] The application of different methods to improve nitrate removal efficiency has been the focus of many review articles. A review conducted by Liu and colleagues[42] discussed the significance of iron in water treatment. This review provides an overview of the current state of iron application in nitrogen removal processes.

The authors discussed the challenges and drawbacks in nitrogen removal processes to achieve practical engineering applications of nitrate removal coupled with iron. A study by Zhang et al.[43] evaluated the removal of ammonium, nitrate, and phosphate from water using biochar and its modified form. After conducting a review study, the authors concluded that biochar modified with metals is more effective in removing pollutants than unmodified biochar. Zou et al.[44] proposed combining electrochemical reduction and anaerobic ammonium oxidation processes to treat nitrate-rich wastewater. In their short review article, the authors discussed the principles, advantages, and problems of this combined method. They found that the combination of electrochemical and anammox technology offers several advantages in nitrate reduction. Zhao et al.[45] discussed different in situ remediation techniques for nitrate remediation in groundwater, including biostimulation, phytoremediation, electrokinetic remediation, etc. The authors also outlined the principles and applications of each in situ remediation, as well as the latest progress, problems, and on-field challenges. They concluded that the combined in situ remediation of groundwater nitrate contamination should be studied continuously. A recent review[46] outlined the advantages of iron-based materials in electrocatalytic nitrate reduction. Among these, single-atom iron catalysts exhibit superior catalytic activity, selectivity, and improved stability compared to other iron-based materials. Many articles have been published on electrochemical nitrate reduction technology over the past decade. The latest review[47] confirms that copper-based electrocatalysts excel as electrochemical nitrate reduction catalysts due to their cost-effectiveness, abundance of raw materials, and high efficiency in nitrate adherence and decomposition. The solid-phase denitrification technique has also shown promise in the elimination of biological nitrate.[48] Carbon sources, temperature, dissolved oxygen levels, and superficial hydraulic velocity influence the denitrification rate, effluent quality, and nitrite accumulation. Lazaratou et al.[49] compiled existing research on using clays for nitrate adsorption from water, emphasizing the underlying mechanisms. The authors suggested that field trials and pilot-scale experiments are critical to the success of the proposed treatment processes. In a kind of analytical review, the cost-effectiveness of different nitrate removal techniques has been evaluated along with suitable policy development to ensure that rural and urban populations receive safe and clean water free of nitrate. By focusing on remediating nitrate from contaminated water samples, Bishayee et al.[50] reviewed the merits and demerits of several remediation techniques for managing nitrate pollution. As a result of such a comprehensive analysis, recommendations regarding the abatement of excess nitrate to ensure clean water supply seem ideal for municipal communities. A review paper[39] examines various surface modification techniques and compares their respective capacities for enhanced nitrate adsorption. The bioelectrochemical system was developed to remove contaminants from wastewater streams in a sustainable manner. An article discusses the state of the art of bio-electroremediation of perchlorate- and nitrate-contaminated waters.[51]
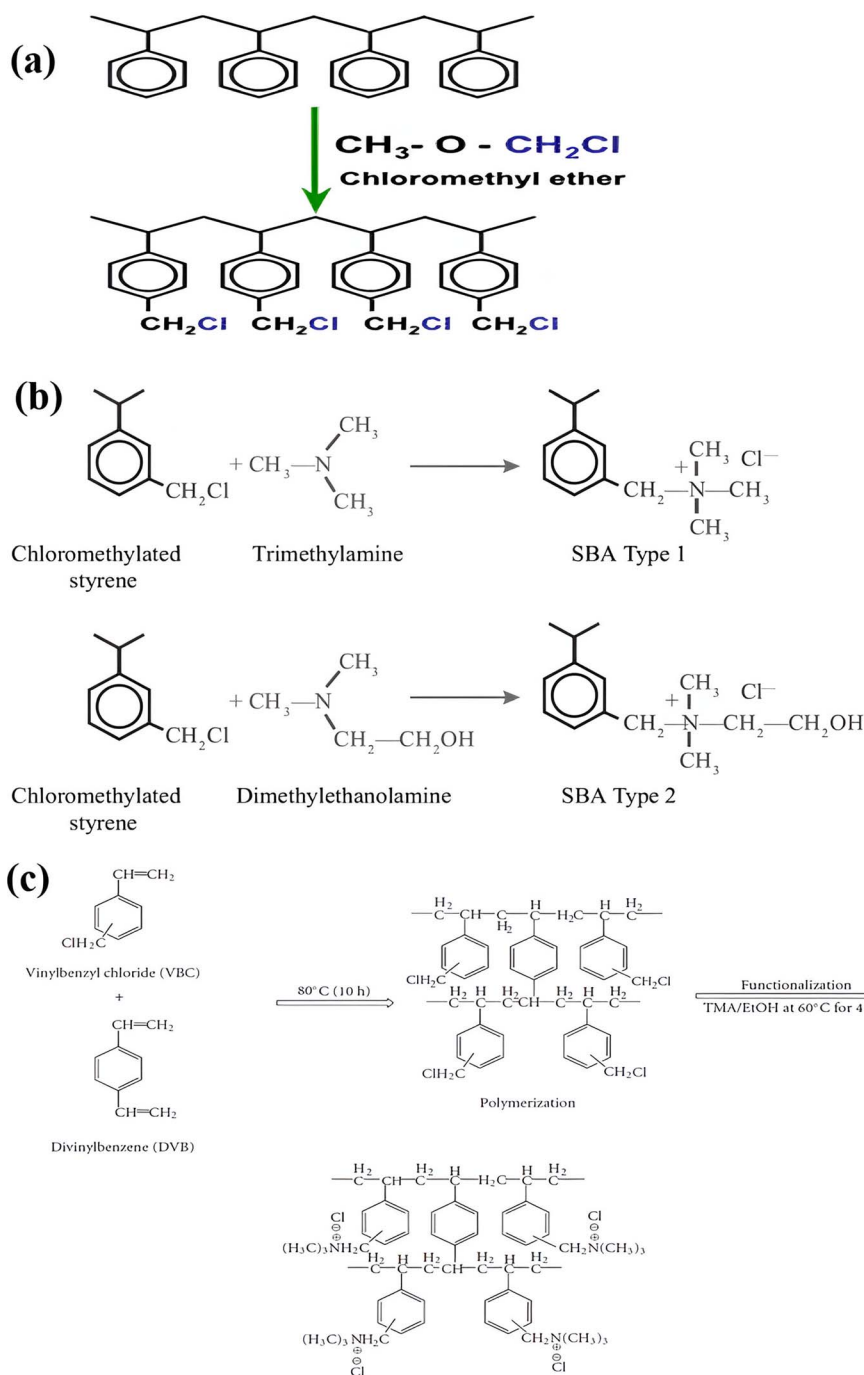
Fig. 1 (a) Chloromethylation,[52] (b) amination,[52] (c) polymerization and functionalization of anion exchange polymer.[53] © François de Dardel 2010–2020 {permission not required}.

3. Synthesis methods

The selection of appropriate methods is based on their efficiency in producing anion exchange resin (AER) with controlled structures using sophisticated and advanced technology.

3.1 Polymerization method

The synthesis of ion exchange resins involves two steps. First, a cross-linking is established between two polymers, and then an ion (anion or cation) is introduced to produce an acid or a base exchange site on the resin. By crosslinking hydrocarbon chains together, ion exchange resins are generally formed by polymerization processes. The cross-linking method provides strength, large volume capacity, and porous structure to the resin polymer. Polystyrene, or cross-linked styrene, is commonly found in ion-exchange resins, while acrylic is also frequently used. As part of the synthesis process, the resin polymer, for example, polystyrene, undergoes a series of
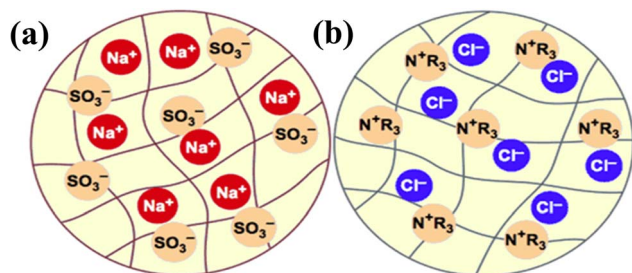
Fig. 2 Schematic cation (a) and anion (b) resin beads[54,55] {permission not required}.

Fig. 3 Synthesis routes (a) grafting-to, (b) grafting-from, (c) grafting through[61] {permission not required}.

chemical reactions, including chloromethylation (Fig. 1a),[52] amination with dimethylamine, and cross-linking with divinylbenzene as shown in (Fig. 1b),[52] to add functional groups to the ion exchange sites within the matrix. Fig. 1c[53] illustrates the AER derived from copolymerized chloromethyl styrene. Various ammonium or ammine groups are found in AER. Each of these functional groups has a different ion-exchange capability, and each type of resin has different exchange abilities. There are two types of AER: type-1 contains tetramethylammonium chloride $-N^+Cl^-$ $(CH_3)_4$ and yields chloride ions (Cl^-) (Fig. 2a),[54,55] while type-2 contains dimethylethanolamine $-N^+(CH_3)_2C_2H_4OH$ and yields hydroxide ions (OH^-) (Fig. 2b).[54,55] Song et al. prepared magnetic polyacrylic AER by polymerization, ammonolysis, and alkylation using divinylbenzene, methyl acrylate, and γ-modified Fe_3O_4 and SN-200, followed by quaternization with N,N-dimethyl-1,3 propane diamine and monochloromethane.[56] Alikhani et al.[57] have synthesized anion-exchange vinyl benzyl chloride/divinylbenzene polyHIPE membranes by high internal phase emulsion polymerization. Abbasian et al.[58] developed anion-exchange macroporous beads using suspension polymerization, wherein chloromethylated PS-DVB copolymers underwent amination via two distinct methods. These bifunctional resins featured two separate ion exchange sites, enhancing selectivity, sorptive capacity, and exchange kinetics. Ghaderi et al.[59] used concentrated emulsion polymerization to synthesize anion-exchange resin from cross-linked polystyrene-divinylbenzene.

3.2 Grafting method

Grafting is the chemical process of synthesizing a polymer chain whose linear backbone chain is covalently bonded to randomly distributed branches of different polymer segments. In general, the grafting process is used to make materials whose branches are chemically different from the primary polymer chain.[60] As a result of the grafting process, ion exchange membranes have a wide range of selectivity, resistance, and mechanical and thermal properties. According to the types of branches and chemical compositions, the synthesis route can be categorized as grafting to (Fig. 3a),[61] grafting from (Fig. 3b),[61] or grafting through (Fig. 3c).[61] The process of "grafting-to" is a combination of synthesizing nanoparticles and polymers separately, then linking them together, with the end-functionalized polymer reacting with the nanoparticles. Using the "grafting-from" method, polymer chains are synthesized
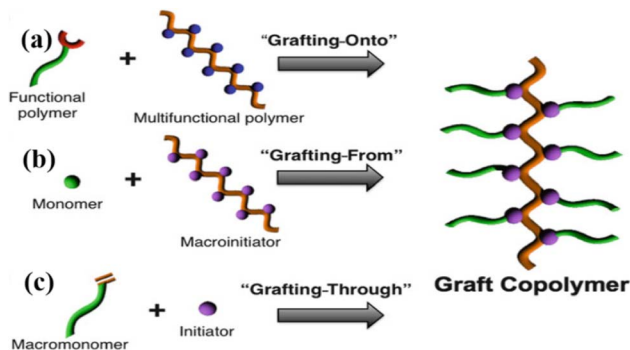
from initiators attached to the surface of nanoparticles. Finally, in the "grafting-through" method, polymerizable groups are added to the nanoparticle surface. All three processes are depicted in Fig. 4a–c.[62] In the next step, polymerization begins in a solution containing an initiator, monomers, and modified nanoparticles, which act as crosslinkers.

3.2.1 Grafting-to. The grafting-to method entails the nucleophilic coupling of anionic polymer chain ends to a multifunctional polymer that possesses functional groups such as halides, esters, and others. Grafting-to generally involves chemical modification of the backbone, but natural polymers can also be used to incorporate functional groups.[63] Condensation and "click" chemistry reactions are the two most often used within this approach.

3.2.2 Grafting from. The grafting-from technique involves controlled polymerization, which is initiated by introducing multiple initiating groups to a backbone polymer. This backbone polymer is synthesized from functional monomers that have initiating groups added to the precursor, thereby forming the graft copolymer. The grafting-from method is advantageous because the side chains are densely introduced. Polyethylene, polyvinylchloride, and polyisobutylene have been used as catalysts for the grafting-from techniques.[64–66]

3.2.3 Grafting through. "Grafting-through" is a simple and facile method for synthesizing graft copolymers with well-defined side chains. Various macromonomers can be synthesized by introducing a polymerizable functional group on the
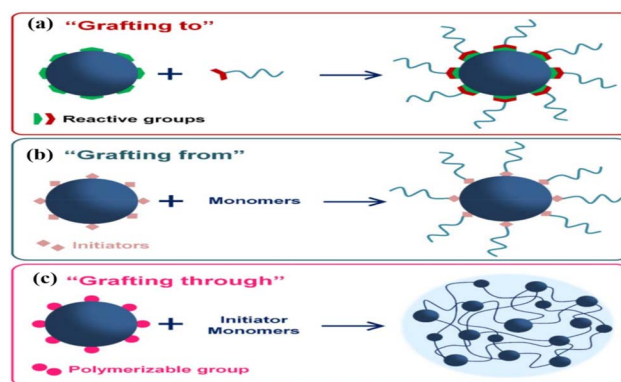

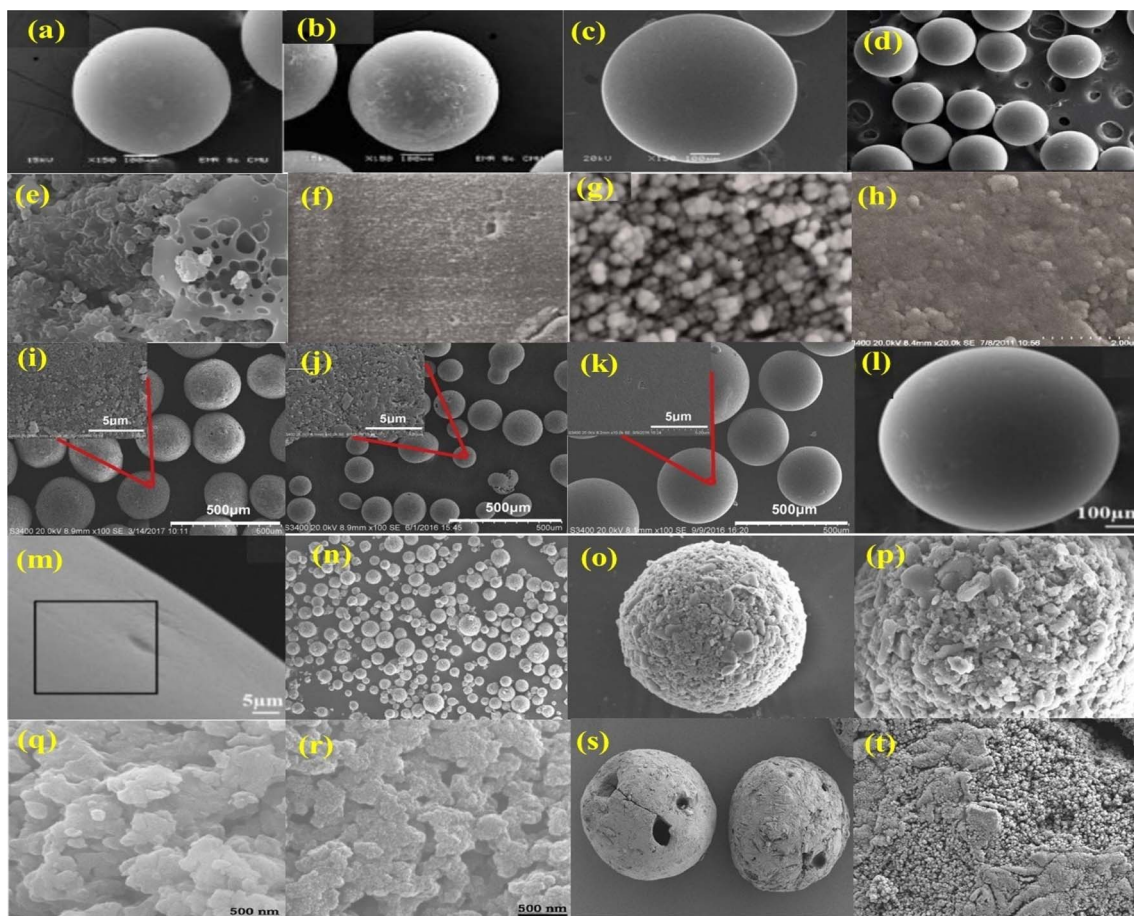Fig. 4 Grafting synthesis process (a) grafting-to, (b) grafting-from, (c) grafting-through[62] {permission not required}.

Fig. 5 SEM images of anion exchange resins (a) Dowex,[70] (b) FO-Dowex,[70] (c) De-Acidite FF-IP {reproduced from ref. 71 with permission from Elsevier (License number-55312502299948)}. (d) nZVI-402-Cl {reprinted (adapted) with permission from ref. 72 Copyright © 2022 American Chemical Society}. (e) PVC-based anion exchange resin {reproduced from ref. 73 with permission from Elsevier (License number-5531290655343)}, (f) polymeric anion exchanger {reproduced from ref. 74 with permission from Elsevier (License number-5531291287322)}, (g) polymeric anion exchanger decorated with magnetite nanoparticles {reproduced from ref. 74 with permission from Elsevier (License number-5531291287322)}, (h) NDP-2 resin {reproduced from ref. 75 with permission from Elsevier (License number-5531260219427)}, (i) L-20 resin {reproduced from ref. 76 with permission from Elsevier (License number-5533211402968)}, (j) ML-20 resin {reproduced from ref. 76 with permission from Elsevier (License number-5533211402968)}, (k) MIEX resin {reproduced from ref. 76 with permission from Elsevier (License number-5533211402968)}, (l) D201 resin {reprinted (adapted) with permission from ref. 77 Copyright © 2020 American Chemical Society}, (m) D201 resin after NO_3^- adsorption {reprinted (adapted) with permission from ref. 77 Copyright © 2020 American Chemical Society}, (n–p) MAER resin {reproduced from ref. 56 with permission from Elsevier (License number-5530880464787)}, (q and r) the Purolite A520E resin, magnetic resin {reproduced from ref. 78 with permission from Elsevier (License number-5794900244372)}, (s and t) MGE resin {reproduced from ref. 79 with permission from Elsevier (License number- 5794890063873)}.

polymer's terminal. Various macromonomers have been incorporated into polystyrene backbones, including polyethylene,[67] polysiloxanes,[68] polycaprolactone,[69] *etc.* The grafting-through approach *via* free radical polymerization has been popular because of its simplicity and cost-effectiveness.

4. Characterization techniques

4.1 Scanning electron microscopy (SEM)

In the field of microscopic analysis, SEM is one of the breakthroughs when it comes to solid microstructures and bulk materials. Based on SEM observations, AER have spherical and smooth surfaces according to many studies. In one study,[70] a material called FO-Dowex was prepared by adding iron oxide

to a strong base AER *i.e.* Dowex marathon MSA. SEM images of Dowex marathon MSA reveal its uniform and smooth surface (Fig. 5a), while FO-Dowex is rough due to iron oxide deposition (Fig. 5b).[70] SEM micrographs of polystyrene-based strongly basic AER *i.e.* De-Acidite FF-IP also show sphere-shaped and smooth resin granules (Fig. 5c).[71] In another study,[72] SEM micrographs of the nanoscale zero-valent iron confined in Alfa Aesar Amberlite ion-exchange resin-402 composite (nZVI-402-Cl) indicate a smooth surface (Fig. 5d). In the latest study of PBE-8 AER, Ren *et al.*[80] found that the magnification of the resin's particles at 50, 2000, and 10 000 times was composed of spheres with uniform holes distributed throughout. PA202 resin showed a uniform, spherical morphology without crushed pearls. Polymer beads had diameters ranging from 0.4 to 1 mm.[81]

Similarly, an SEM image of polyvinylchloride (PVC) based anion exchangers shows smooth surfaces of the plasticized PVC (Fig. 5e).[73] As shown in Fig. 5e, a porous granule results from the extraction of plasticizer and the introduction of amine groups. It indicates that the PVC-based anion exchanger has a large surface area. Based on its morphological structure, the material appears to be highly adsorbent. SEM images of a polymeric AER show that the resin beads are smooth and flat (Fig. 5f),[74] while when it was decorated with magnetite nanoparticles, Fig. 5g clearly shows magnetite nanoparticles agglomerated to a high degree. It was estimated that polymeric resin beads have an average diameter of 75 millimeters.[74] It can be seen that AER *i.e.* NDP-2, has more uniform planar surfaces (Fig. 5h).[75] Moreover, the latest study[82] reveals that AER *i.e.* A520E exhibited a rich porosity structure inside, as well as a flat and smooth surface.

In some studies, however, an irregular, rough, and hard surface morphology was found on the AER. The surface morphologies of polystyrene AER, *i.e.* L20 resin (Fig. 5i),[76] a PS resin that was aminated by trimethylamine, synthetic magnetic ML20 resin (Fig. 5j),[76] and commercial MIEX resin modified by epoxy groups (Fig. 5k)[76] have satisfactorily monodisperse properties and ranged in size from 80 to 250 mm, about three to seven times smaller than conventional resins. There is only one explanation for the rough surfaces of these resins: needle-shaped g-Fe_2O_3, which provides more adsorption sites.[76] The morphology of AER *i.e.* D201, a strong base Type I macroporous AER containing quaternary ammonium as the functional group is shown before (Fig. 5l)[77] and after nitrate adsorption (Fig. 5m).[77] Compared with the virgin D201 resin, the resin's surface was roughened after adsorption.[77] The macroporous magnetic acrylic strong AER *i.e.* MAER contains sheet-shaped γ-MPS modified Fe_3O_4 which aids in the creation of rough surfaces (Fig. 5n–p).[56] As compared to conventional resins, MAER exhibited a size of 0.05–0.12 mm, which was about 6–8 times smaller.[56] Comparative analysis of the primary resin and magnetic resin surfaces revealed that the primary resin's surface is regular and smooth (Fig. 5q).[78] In contrast, the magnetic resin showed that Fe_3O_4 nanoparticles adhere to the surface as tiny particles, resulting in increased surface roughness and magnetization (Fig. 5r).[78] SEM images revealed spherical beads with rough and porous surfaces within a magnetic AER *i.e.* MGE (Fig. 5s and t).[79] As a result of all the above analysis, it is determined that the surface of AER is smooth before modification or treatment and that it becomes rough afterward.

4.2 Energy dispersive X-ray (EDX) analysis

The EDX analysis of commercial strong base AER *i.e.* Dowex anion resin and an adsorbent (FO-Dowex) prepared by modification of Dowex anion resin with ferric oxide is illustrated in Fig. 6a.[70] Dowex anion resin is found to contain mainly carbon and chlorine, likely as a result of its polymeric matrix and exchangeable ions. As for FO-Dowex element compositions, Fe (53.24% wt) is detected.[70] The same type of result was obtained
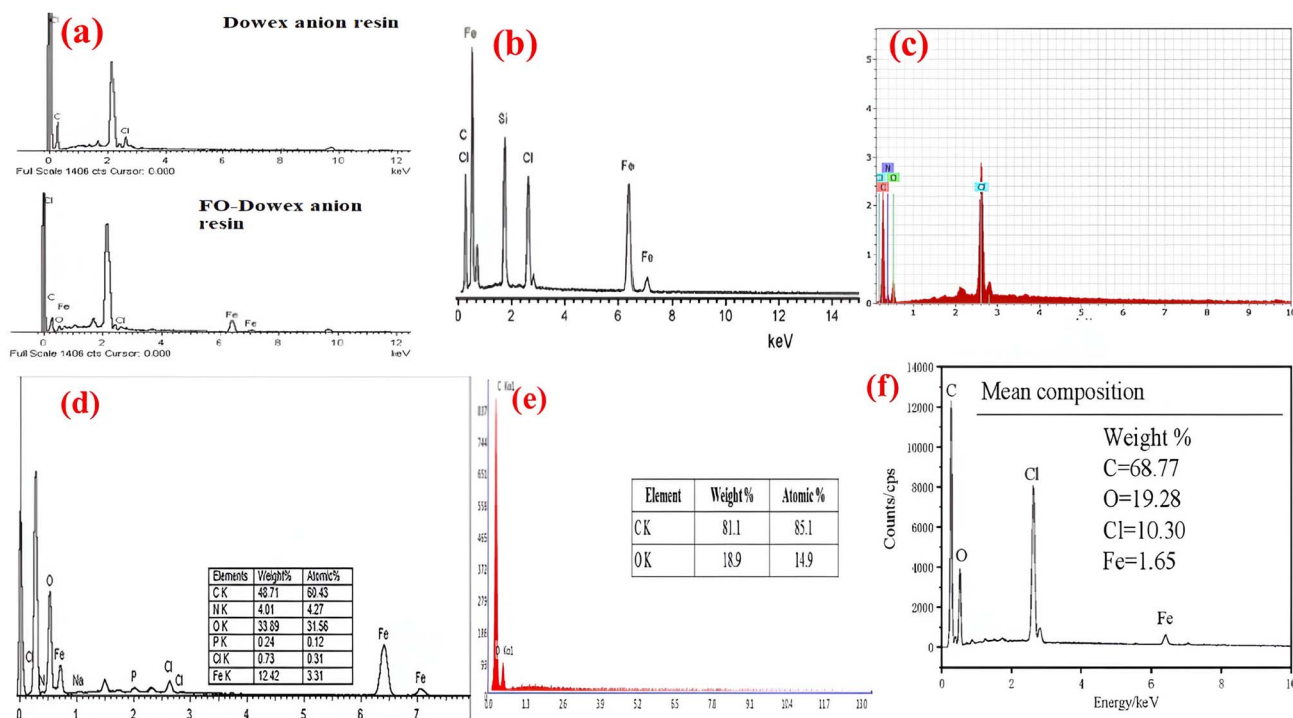

Fig. 6 EDX spectra of anion exchange resin (a) FO-Dowex,[70] (b) magnetic anion exchange resin,[83] (c) QCMGR {reproduced from ref. 84 with permission from Elsevier (License number-5543001457001)}, (d) R$_4$N$^+$ {reproduced from ref. 85 with permission from Elsevier (License number-5531310164816)}, (e) strongly basic anion exchange resin (reproduced from ref. 86 Copyright © 2014 Académie des sciences. Published by Elsevier Masson SAS All rights reserved) (f) nZVI-402-Cl[72] {reprinted (adapted) with permission from ref. 72 Copyright © 2022 American Chemical Society}.

for a magnetic AER with a polyacrylic matrix in which EDX analysis confirms the existence of iron and silicon (Fig. 6b).[83] The EDX spectra Fig. 6c confirmed that the basic constituents of the quaternized chitosan–melamine–glutaraldehyde resin (QCMGR) were carbon, oxygen, nitrogen, and chlorine.[84] The EDX spectra of the triethylamine functionalized strong base anion resin (R_4N^+) indicate a 12.42% mass loading rate of iron onto the polymeric ion exchangers (Fig. 6d).[85] When EDX data are analyzed before and after NO_3^- adsorption experiments on Purolite A-520E, it is apparent that the resin's initial matrix contains carbon, nitrogen, oxygen, and chloride (Fig. 6e).[86] When the resin came into contact with NO_3^--containing solutions, the intensity of the chlorine peaks experienced a substantial decrease.[86] Based on the iron content in the core of the nZVI-402-Cl composite, Fe_3^+ diffused into the resin particles, allowing for the formation of the nanoscale zero-valent iron inside, providing the expected protraction against fast oxidation during adsorption by the surrounding environment (Fig. 6f).[72] When comparing the EDX analysis of Purolite A520E resin and iron oxide-modified Purolite A520E resin, it is evident that carbon, chlorine, oxygen, and iron peaks were observed in the magnetic resin. This suggests the presence of iron nanoparticles in the resin.[78] An elemental composition analysis of MGE indicates a consistent distribution of C (64.20%), O (31.12%), Fe (1.80%), and N (2.88%), with C and O being the primary elements.[79]

5. Adsorption studies

5.1 Effect of pH

The pH of water is a significant environmental factor that impacts most chemical and biological processes. If a waterbody's pH is below 6.0 or 6.5, it is considered to have a low pH. Many factors can cause low pH, such as mine wastes, acidic fumes, industrial effluents, landfill leachate, dairy runoff, etc.[87] When the pH of a water body exceeds 9.0 for an extended period, it is considered to have a high pH. Many factors can cause high pH, such as industrial discharges, agricultural lime, cement and soap manufacturing, industrial landfills, etc.[87] It is possible to determine whether adsorption is desirable in acidic or basic solutions based on the properties of the adsorbent and analyte. Most studies reveal that the sorption of NO_3^- onto AER is not strongly influenced by pH and the solution pH has only a negligible effect on sorption efficiency. As per the results, since AER do not depend on pH, they are especially useful in water treatment, where the pH of the water may vary at altered sites. As this property of the resins facilitates the wide application of water treatment, it is useful also for in-field tasks. For example, different AER prepared from lignocellulose materials
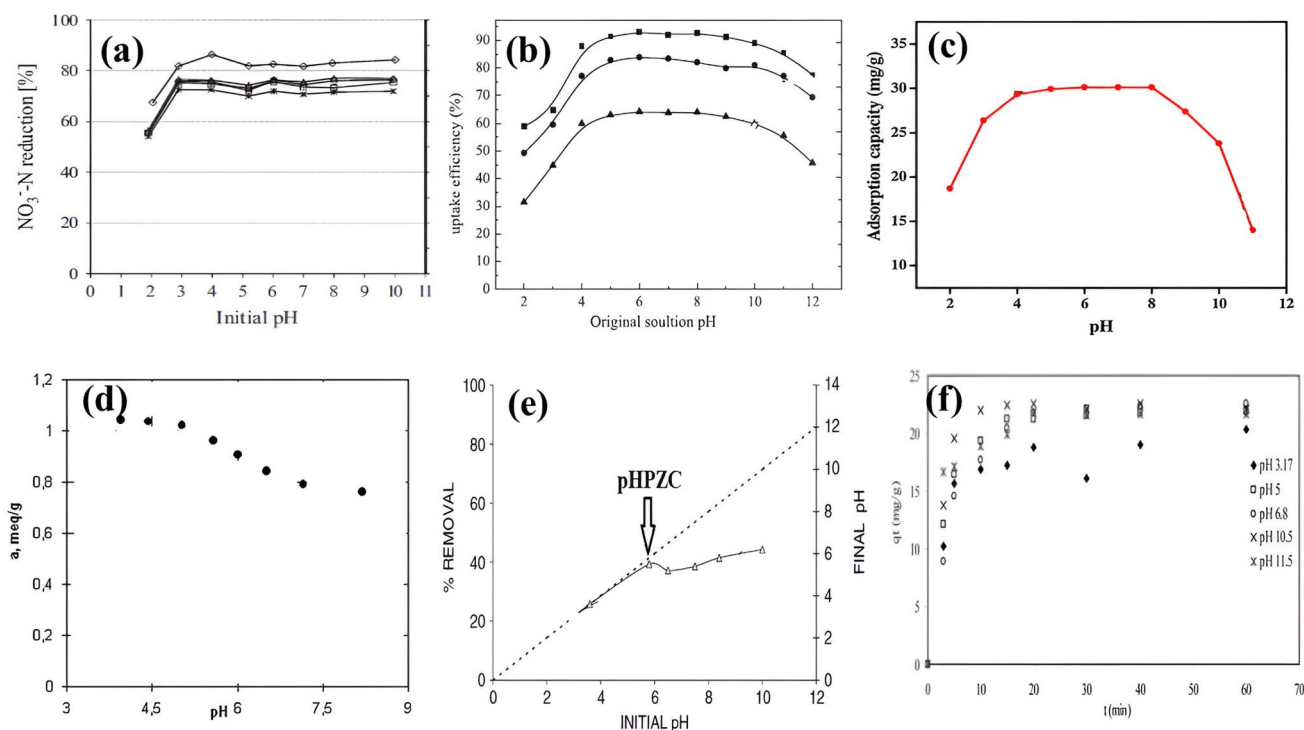

Fig. 7 Effect of pH on nitrate adsorption using (a) anion exchange resins prepared from lignocellulose materials {reproduced from ref. 88 with permission from Elsevier (License number–5531310470709)}, (b) WS-based anion exchange resins {reproduced from ref. 89 with permission from Elsevier (License number–5531310602472)}, (c) chitosan grafted quaternized resin {reproduced from ref. 90 with permission from Elsevier (License number–5531310830204)}, (d) strongly basic anion exchange resin (reproduced from ref. 86 Copyright © 2014 Académie des sciences. Published by Elsevier Masson SAS All rights reserved), (e) quaternized biomass anion exchanger {reproduced from ref. 91 with permission from Elsevier (License number–5531310966038)}, (f) Amberlite IRA 400 resin {reproduced from ref. 92 with permission from Elsevier (License number–5531311174458)}.

give similar adsorption patterns between pH 3–10 (Fig. 7a).[88] In addition, a similar pH range was found to be optimal for NO_3^- sorption on quaternized chitosan–melamine–glutaraldehyde resin.[93] For three polymer-based anion exchange fibers, sorption efficiency was constant in the pH range of 2.0–11.0.[94] Another study[89] found that pH 2.0 to 4.0 led to a sharp increase in % sorption, followed by a plateau at pH 5.0 to 10.0 (Fig. 7b). For the hybrid polymeric anion exchanger containing triethylamine functional groups and iron oxide nanoparticles, in a pH (3.0–11.0), sorption values of NO_3^- varied marginally between 56.85 and 60.37 mg g^{-1}.[85] The reason for the constant NO_3^- sorption under a wide pH range was given by Wiriyathamcharoen *et al.*[85] by stating that nitrate ions were capable of forming conjugates with acids, including nitric acid, and thus remained ionized throughout all pH values and therefore have a constant affinity for ion exchange functional groups. Milmile *et al.*[95] also concluded that since the resin did not contribute protons to the solution and hence the solution pH remained unaffected. Therefore, NO_3^- adsorption was not affected either. Sun and Zheng[94] suggested that the electrostatic attraction between the positively charged fiber surface and the anionic NO_3^- species may cause the adsorption to occur in a stable form. Öztürk *et al.*[96] reported that the pH values didn't alter the NO_3^- adsorption from aqueous solutions for any adsorbent other than activated carbon. Li *et al.*[76] observed negligible differences in NO_3^- adsorption in the pH range of 3.0–11.0. Since anions are mainly absorbed by electrostatic interactions or Columbia forces, and the zeta potentials of the tested anion exchange resins could remain stable under an acidic and basic environment, the adsorption of NO_3^- remained constant, mainly because the resin matrix contained quaternary ammonium groups. Four different biomaterial-based resins were tested by Xu *et al.*,[97] and they found that their activities were independent of pH (4–10) which enabled their wide application. The most recent study[98] also showed that the adsorption capacity of novel strong anion exchangers showed no significant change across a broad pH range (2.0 to 12.0), except pH 2.0, where the adsorption capacity initially increased and then decreased upon approaching neutral pH levels.

However, some other studies have noted a decrease in NO_3^- adsorption at higher pH ranges. According to the authors,[90] the adsorption capacity of adsorbent for NO_3^- ion decreased at higher pH due to competition between the OH^- ions and the NO_3^- ions (Fig. 7c). Similarly, other authors found[93] that the noteworthy lessening in NO_3^- adsorption after pH 10 was caused by OH^- ions. In addition, the OH^- concentration increased significantly as the pH value increased beyond 10.0, and the binding sites for NO_3^- uptake decreased on the surface of the resins because of the competition between excess OH^- ions and the nitrate ions for exchange sites.[89] The optimum sorption on De-Acidite FF-IP resin for various NO_3^- at various concentrations was observed at pH 2. A gradual decrease in NO_3^- sorption occurred until pH 6 and a drastic decrease occurred between pH 6 and 8.[71] It was caused by the same reason as stated above. The adsorption capacity of the Purolite A-520E resin decreased when the pH value increased between

3.9 and 8.2 (Fig. 7d).[86] As a result of the chemical process, chloride ions from resin were exchanged with nitrate ions from aqueous solutions. At low pH values, hydroxyl anion concentrations were low and nitrate ions were more readily absorbed. A higher pH value resulted in a greater amount of hydroxyl ions and a greater number of active centers.

The point of zero surface charge (pH_{pzc}) is a key parameter for understanding how pH affects the sorption process. As the pH value of the solution was changed from 1 pH to 13 pH, the authors examined the NO_3^- adsorption effect of the adsorbents and pH_{pzc} of the adsorbents.[99] It was observed that the removal efficiency of NO_3^- increased as pH increased, reaching the maximum value at pH 5, then gradually declining. As a result of measuring the pH difference, this adsorbent was calculated to have a pH_{pzc} of 6.09. This indicates that when the pH of the adsorbent was greater than 6.09, the adsorbent's surface was negatively charged and when the pH of the adsorbent was less than 6.09, the adsorbent's surface was positively charged. In alkaline environments, the adsorption efficiency decreased due to the negatively charged adsorbent's surface and competitive adsorption resulting from the production of OH^-.[99] In another study,[100] pH_{pzc} of Fe–Mg/CER material was 7, and therefore, at pH < 7, anion was adsorbed *via* electrostatic attraction. On the contrary, pH > 7 resulted in negatively charged surfaces, which were not suitable for NO_3^- adsorption. Additionally, the adsorption capacity was reduced because OH^- ions competed for surface positions inhibiting the adsorption of anions such as nitrate. According to another study,[91] by raising the pH above 6.0, the number of negatively charged adsorbent sites increased, and this resulted in a slight decrease in nitrate adsorption due to electrostatic repulsion (Fig. 7e). It was found that the nitrate adsorption capacity increased from 53.45 mg g^{-1} to 75.17 mg g^{-1} at pH 4.0–6.0 but decreased gradually at pH 7.0–10.0. When the pH rises to an alkaline level, OH^- and NO_3^- compete for active sites.[79]

The result of one study,[92] however, was diverse as the highest adsorption capacity of Amberlite IRA 400 resin towards NO_3^- was obtained at pH 10.5 and a significant decline in adsorption capacity was observed as the pH value decreased (Fig. 7f). It has been suggested that this may be caused by the dissociation of the adsorbent's functional groups at acidic pH, which could produce an electrostatic binding with negatively charged nitrates. When pH was increased to the basic range (pH 3.0–11.5), the adsorption was increased.

5.2 Effect of concentration

By increasing the concentration of NO_3^- solution, the impact between NO_3^- ions and the ion exchange resin adsorbents is enhanced, resulting in a greater adsorption capacity. In a study,[56] four initial concentrations (0.805, 1.61, 3.22, and 483 mmol L^{-1}) were investigated using an AER at 293 K, with equilibrium adsorption capacities of 0.37, 0.69, 1.17, and 1.50 mmol g^{-1}, respectively. In another study,[71] during the adsorption process on polystyrene-based AER, the NO_3^- levels increased with the increase in NO_3^- concentration due to increasing concentration gradients with increasing adsorbate
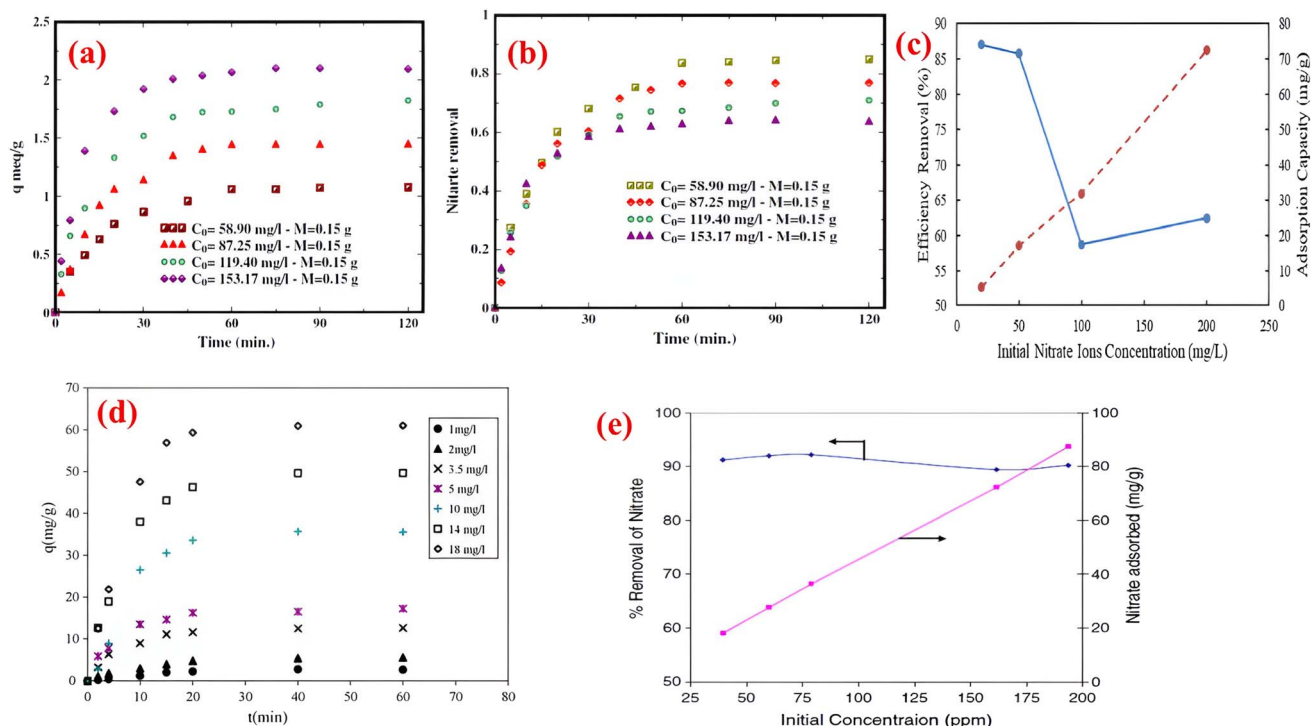
Fig. 8 Effect of concentration on nitrate adsorption using (a–c) anion exchange resin {reproduced from ref. 101 with permission from Elsevier (License number-5531491378704)}, (d) Amberlite IRA 958-Cl resin {reproduced from ref. 102 with permission from Elsevier (License number-5531301463090)}, (e) Indion NSSR resin {reproduced from ref. 95 with permission from Elsevier (License number-5531491232894)}.

concentrations. Initially, low concentrations of NO_3^- led to a rapid increase because there were enough adsorption sites. As the initial concentration of NO_3^- raised, the adsorption sites became increasingly occupied by NO_3^-, leading to saturation.[98]

Fig. 8a and b reflect the time course effect of initial NO_3^- concentration on the amount of adsorption.[101] The study revealed a decrease in removal efficiency as the NO_3^- concentration increased (Fig. 8c).[101] Norhayati *et al.*[102] also found that the adsorption capacity of Amberlite IRA 958- Cl resin increased from 5.4 to 72.5 mg g^{-1} with the rising concentration of NO_3^- ions from 20 and 200 mg L^{-1}, respectively while the efficiency (% removal) of NO_3^- ions removal was decreased from 87 to 59% (Fig. 8d). A high initial concentration of adsorbate molecules at the surface of the adsorbent causes a high mole ratio of adsorbate molecules, which leads to an increase in adsorption quantity.[103,104] When adsorbate concentrations are low, few adsorbate molecules are present, but as concentrations increase, mass transfer forces increase, causing the maximum number of adsorbate molecules to be attracted to the surface.[105–110] An explanation for the decrease in % removal was provided by the authors, who interpreted that the increased ratio of NO_3^- ions from the aqueous solution, as well as the restricted sorption sites on the Amberlite IRA 958-Cl resin surface, were the reasons for the decrease.[102]

Interestingly, in study,[95] it was observed that a slight decrease in NO_3^- adsorption (from around 92 to 90%) occurred as the initial concentration increased (from 40 to 180 mg L^{-1}). As a result, nitrate removal increased linearly, with negligible

effects on total adsorption capacity (mg g^{-1}), as shown in Fig. 8e. Conversely, Hekmatzadeh *et al.*[111] found that initial NO_3^- concentration did not affect the adsorption capacity significantly. Based on their experiments, they found that the amount of adsorbed NO_3^- was in the range of 55.1 to 56.8 mg NO_3^- per mL resin as the initial NO_3^- concentration increased from 60.4 to 119.4 mg L^{-1}. A recent study[112] also supported this outcome which shows that the maximum capacity of NO_3^- adsorption increased by 2% when more NO_3^- concentration was applied, indicating that the initial NO_3^- concentration does not significantly affect the maximum capacity of NO_3^- adsorption.

5.3 Adsorption isotherm

Adsorption isotherm provides a very useful description of the interaction between adsorbate and an adsorbent. Parameters derived from isotherm data modeling could be used for the proper design and analysis of adsorption systems. Several well-known isotherm models of adsorption have been developed by the scientific community, including Langmuir,[113] Freundlich,[114] Temkin,[115] Redlich-Peterson,[115] Elovich Isotherm,[116] Dubinin–Radushkevich,[116] and Sips[117] as summarized in Table 2. The maximum adsorption capacities for NO_3^- adsorption onto AER are summarized in Table 3. There are abundant studies, reported on the fitting of either the Langmuir or Freundlich isotherm models to describe NO_3^- adsorption onto resins. Several studies have reported on the fitness of the Langmuir model with NO_3^- adsorption equilibrium data, such as Keränen

Table 2 Isotherm models, their equations, and parameters

Adsorption isotherm	Non-linear equation	Linear equation
Langmuir	$q_e = \dfrac{q_m K_L C_e}{1 + K_L C_e}$ Where C_e is the equilibrium concentration of the aqueous solution (mg L^{-1}), q_e is the equilibrium capacity (mg g^{-1}), q_m is maximum uptake (mg g^{-1}), and K_L is the Langmuir constant (L mg^{-1})	$\dfrac{1}{q_e} = \dfrac{1}{q_m \times b} \times \dfrac{1}{C_e} + \dfrac{1}{q_m}$
Freundlich	$q_e = K_F C_e^{1/n}$ Where K_F and $1/n$ are the Freundlich constants that suggest the intensity of adsorption and capacity of adsorption, respectively	$\log q_e = \log K + \dfrac{1}{n} \log C_e$
Temkin	$q_{7e} = B_1 \ln(K_T C_e)$ Where B is the value of heat of adsorption, R is the gas constant of the value 8.314 J mol K^{-1}, and K_T is the equilibrium binding constant	$q_e = \dfrac{R_T}{b_T} \ln C_e + \dfrac{R_T}{b_T} \ln K_T$
Dubinin–Radushkevich	$q_e = q_m \exp(-\beta \varepsilon^2)$ Where β is the adsorbate mean free energy per mole, ε is the Polanyi potential. Where q_{DR} is D–R isotherm saturation capacity and β is D–R isotherm constant which gives mean free energy (E) per molecule of the adsorbate of sorption per molecule of sorbate, ε is a temperature-dependent parameter and related as: $\varepsilon = RT$ $\ln(1 + 1/C_e)$	$\ln q_e = \ln q_{DR} - \beta \varepsilon^2$
Elovich	$q_t = \dfrac{1}{\beta} \ln(1 + \alpha \beta_t)$ Where α is the Elovich initial adsorption rate (mg g^{-1} min^{-1}), β (g mg^{-1}) desorption constant	$q_t = \dfrac{1}{\beta} \ln\left(1 + \alpha\beta + \dfrac{1}{\beta} \ln t\right)$
Redlich–Peterson	$q_e = \dfrac{K_{RP} C_e}{1 + a_R C_e^{\beta}}$ Where K_{RP} and β are the R–P constants	$\ln\left(K_{RP} \dfrac{C_e}{q_e} - 1\right) = g \ln C_e + \ln a_R$
Sips	$q_e = \dfrac{Q_s K_s C_e^{n_s}}{1 + K_s C_e^{n_s}}$ Where K_s is the equilibrium constant	$\ln\left(\dfrac{q_e}{q_m - q_e}\right) = \dfrac{1}{n} \ln C_e \ln K_s$

et al. 2013 (ref. 88) who compared both the linear and nonlinear forms of the Langmuir and Freundlich models. They found that the linear Langmuir model has slightly better R^2 values than the nonlinear. A better fit was found with the Langmuir model ($R^2 = 0.93$–0.94) than with the Freundlich model ($R^2 = 0.84$–0.96). Regarding R^2 values, Langmuir's model was also better suited to the D890 macroporous AER adsorption mechanism. This study found that NO$_3^-$ ions were predominantly absorbed through uniform monolayer adsorption at 25 °C unlike the other temperatures examined.[126] It was found that the Langmuir model was more suitable for adsorption studies on magnetic resins than the Freundlich isotherm.[78]

Alternatively, some studies found that the nonlinear Freundlich model was more appropriate for the studied materials *i.e.* new AER prepared from spruce bark, birch bark, and peat.[88] The authors suggested that the adsorption mechanism was based on ion exchange and that monolayer adsorption supported this theory. Chabani *et al.*[92] fitted the experimental adsorption data to the various Langmuir models and found that Langmuir form II provided higher adsorption capacity than form I. They also applied the Frumkin isotherm model which gave satisfactory R^2 values; however, in comparison with the Langmuir model form II, the values were slightly lower. Hence, the adsorption of NO$_3^-$ on Amberlite IRA-400 was monolayered or followed a Langmuir model. Furthermore, the separation factor (R_L) values computed from Langmuir parameters (form II) supported the favorable NO$_3^-$ adsorption independent of the studied initial NO$_3^-$ concentration (2–20 mg L^{-1}). Milmile *et al.*[95] used an AER known as Indion NSSR and found that the

linear isotherm plot of Langmuir model was better fitted. However, the plot of the Freundlich model was also linear, indicating favorable adsorption, but the adsorption capacity (q_e) values were lower than those from Langmuir. According to Sun and Zheng,[94] the Langmuir model was found more appropriate for explaining the adsorption isotherms of the polyacrylonitrile anion exchange fiber than the Freundlich model, as defined by R^2 values. While using a monolithic AER *i.e.* PolyHIPE it was observed that the Langmuir model was more appropriate for analyzing NO$_3^-$ adsorption equilibrium data.[127]

On the other hand, several studies reported that NO$_3^-$ adsorption on resins could be well represented by Freundlich rather than Langmuir isotherm model. For example, Song *et al.*[56] found that the Freundlich model represented the results more accurately than the Langmuir model, which suggested that the surface of magnetic polyacrylic AER for NO$_3^-$ adsorption was heterogeneous. In addition, the authors compared the Langmuir and Freundlich isotherm parameters and concluded that the studied magnetite AER was among the best for adsorption of NO$_3^-$. Naushad *et al.*[71] used non-linear plots to demonstrate the applicability of the Freundlich model. They observed high R^2 values in conjunction with low error function values and explained that NO$_3^-$ adsorption on cross-linked polystyrene-based strongly basic AER occurred on a heterogeneous surface and displayed multilayer adsorption properties. Also, another study[57] showed that the equilibrium data fitted well with the Freundlich model compared to the Langmuir and Temkin models. By studying two AER of Purolite (A500PS and A520E), Nur *et al.*[128] found that in batch equilibrium adsorption

Table 3 Maximum adsorption capacities for nitrate adsorption onto various anion exchange resins

Adsorbent	Maximum adsorption capacity, q_m (mg g^{-1}) as calculated by Langmuir isotherm	Experimental conditions (dose: g/concentration: mg L^{-1})	Reference
MLC resins – Mod. pine sawdust	31.55	3/30	88
MLC resins – Mod. pine bark	26.50	3/30	88
MLC resins – Mod. spruce bark	27.70	3/30	88
MLC resins – Mod. birch bark	28.03	3/30	88
MLC resins – Mod. peat	27.36	3/30	88
Amberlite IRA 400-macroporous anion-exchange resin	65.36	2/15	92
Anion exchange Indion NSSR resin	119.30	2/100	95
NDP-2	174.20	1/100	75
Commercial anion exchange resin, Purolite A 300	147.41	1/100	75
Commercial anion exchange resin, D201	173.80	1/100	75
Polyacrylonitrile anion exchange fiber PAN-PEI-3C	31.30	0.1/20	94
Polyacrylonitrile anion exchange fiber PAN-PEI-5C	31.32	0.1/20	94
Polyacrylonitrile anion exchange fiber PAN-PEI-8C	31.19	0.1/20	94
WS resins	89.80	4/100	89
Amberlite® IRN 9766 strong anion exchanger	190.60	0.05/—	118
Wheat straw anion exchanger	52.80	35/—	119
Purolite A 520E	81.97	3/100	120
Amberlite IRA 400	769.20	2/15	121
Purolite A500P anion exchange resin	64.00	10/50	122
Quaternized biomass of Chinese reed	7.55	0.4/10	91
Purolite A520E	32.20	1.5/20	123
Commercial anion exchange membrane-AFN membrane	2.66	—/50	124
Pilot-scale produced wheat stalk resin	43.88	2/50	97
Pilot-scale produced cotton stalk resin	33.35	2/50	97
Lab-scale produced wheat stalk resin	50.24	2/50	97
Lab-scale produced cotton stalk resin	39.15	2/50	97
Polyacrylic anion exchange resin	40.32	0.2/60	125
Purolite A-520E resin	129.87	—/2.1 mequiv.	86

experiments, Freundlich and Langmuir isotherm models fitted well for the adsorption of NO$_3^-$ on A520E, with R^2 ranging from 0.95–0.96. NO$_3^-$ adsorption on A500PS, however, could be satisfactorily described only by a Freundlich model ($R^2 = 0.98$).

The equilibrium data of NO$_3^-$ sorption on AER were also found to fit equally by the Langmuir and Freundlich equations in some studies. By using dried Chinese reed as an anion exchanger, Namasivayam and Höll[91] developed equilibrium adsorption data for NO$_3^-$ removal that followed both Langmuir and Freundlich isotherms. Using a macroporous AER, Song et al.[75] also showed that the Freundlich and Langmuir adsorption isotherms were both suitable for NO$_3^-$ removal. A recent study[79] demonstrated that the removal of NO$_3^-$ by MIEX® (magnetic AER and D201-type I AER) closely aligned with the Langmuir isothermal equations, showing R^2 values of 0.991 and 0.992, respectively. By contrast, MGE showed better agreement with the Freundlich model ($R^2 = 0.980$) for NO$_3^-$ removal.

Dron and Dodi (2011)[118] compared different equilibrium models for NO$_3^-$ adsorption by an AER. They found that Langmuir's isotherm matched experimentally well, and Freundlich's isotherm also showed favorable adsorptions in the same order of affinity as Langmuir's isotherm. Compared to the Freundlich model, the Langmuir model performed better in the high-concentration range. Furthermore, they also used Dubinin–Radushkevitch (D–R) and Dubinin–Astakhov (D–A) isotherm models and found that the adsorption energies calculated from both isotherms, especially D–A, agreed well. After comparing the results of both models, the authors concluded that the D–R model presented the best fit for both low-energy ion exchange systems, while the D–A model provided the best fit for the other studied four systems.

In the equilibrium modeling of NO$_3^-$ adsorption, Hekmatzadeh et al.[111] used column mode experiments and applied the mass action law approach and Langmuir model, and found that both models had high R^2 values. According to the authors, there was a lack of accuracy in Langmuir's model equation when it came to predicting the dynamic behavior of resin-filled ion exchange columns, and the mass action law was better than the Langmuir equation since the results revealed the Langmuir constant altered substantially in NO$_3^-$ solutions, while the mass action constant remained nearly constant.

The values of maximum adsorption capacity (mg g^{-1}) of various materials are shown in Table 4, which proves that AER as adsorbents are superior to the materials reported previously and have a practical and viable application for the removal of NO$_3^-$ ions from industrial wastewater.
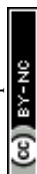
Table 4 Comparison of adsorption capacity of various materials for NO_3^-

Adsorbent	Maximum adsorption capacity (mg g^{-1})	Reference
Amberlite IRA 400	**769.20**	121
Modified sugarcane bagasse biochar	28.21	129
CNTs@AC hybrid material	14.59	130
Bio-graphene nanosheet	182.50	131
Magnetic Mg/Fe hydrotalcite	7.89	132
Glycyrrhiza glabra residue	142.50	133
Biochar-supported Al-substituted goethite	96.14	134
Fe–Zr–chitosan	10.60	135
Montmorillonite clay	89.20	136
Calcined hydrotalcite	34.36	137
Amine-enriched composite	137.62	138
Calcined-layered double hydroxides (Mg3P10-500)	45.47	139
Calcined-layered double hydroxides (Zn3P10-500)	34.34	139
Ammonium-functionalized mesostructured silica	46.00	140
Chitosan hydro beads	92.10	141
Zinc chloride-treated activated carbon	1.70	142
Activated carbon prepared from treated rice husk	70.20	143
Activated carbon prepared from shrimp shell	5.58	144
Chemically activated granular activated carbon	7.3	145
Nano zero-valent iron/biopolymer composite	833.33	146
Polypyrrole-modified plastic-carbon	45.18	147
Oxidized commercial carbon AG-5	0.80	148
Modified hazelnut shell	25.79	149
Hydrogel-based ion-exchange resin (poly(ethylene glycol)diacrylate methacryloxyethyltrimethyl ammonium chloride)	13.66	150
Hydrogel-based ion-exchange resin (poly(ethylene glycol)diacrylate 2-aminoethyl methacrylate hydrochloride)	11.24	150
Graphene	89.97	151
Propylammonium functionalized mesoporous silica material	45.00	152
Green iron oxide nanoparticles synthesized by Eucalyptus leaf extracts	12.91	153
Polystyrene adsorbent functionalized with triethylamine groups	44.92	77
Modified zeolite	24.45	154
PAN-oxime-nano Fe$_2$O$_3$	25.89	155
Modified kaolin	109.89	156
Olive mill residues	110.00	157
Modified maize stalks	232.55	158
Granular activated carbon	81.07	159
FeMgMn-LDH	10.56	160
Surfactant-modified halloysite nanotubes	47.40	161

6. Adsorption mechanism

Since NO_3^- is a monovalent anion, it can be adsorbed on positively charged surfaces or surfaces containing exchangeable ions through electrostatic attraction. In addition to having a large double bond, NO_3^- possesses a four-electron double bond, making the surface of an adsorbent that contains a double bond a potential site for NO_3^- adsorption using π–π attraction. Additionally, the oxygen atoms in NO_3^- molecules possess strong electronegativity, forming hydrogen bonds that create potential adsorption sites for nitrates.[40] NO_3^- adsorption mechanism includes electromagnetic interactions, ion exchange, hydrogen bonding, and complexation which are dependent on the composition, structure, and properties of the adsorbent's surface and the experimental conditions. Fig. 9a shows the possible adsorption sites for NO_3^- adsorption and their resultant adsorption mechanism.[40] In NO_3^- adsorption onto MAER, amine groups were involved in NO_3^- adsorption.[56]

Adsorption occurred through ion exchange by Cl^- displacement. The authors[56] found in the FTIR spectrum of NO_3^- adsorbed MAER a strong adsorption band at 3361 cm^{-1} associated with hydroxyl groups disappeared. The existence of hydrogen bonds between hydroxyl and nitrate groups indicated that hydrogen bonding has occurred in the adsorption mechanism. The hydration energy of ions was taken an account for the adsorption mechanism of NO_3^- by NDP-2 AER. Usually, ion exchange is more favorable with lower hydration energy. The hydration energy of nitrate (-314 kJ mol^{-1}) was lower than that of Cl^- (-363 kJ mol^{-1}) and SO_4^{2-} (-1103 kJ mol^{-1}). Therefore, it can be assumed that the NDP-2 resin favorably absorbed NO_3^-, and the major adsorption mechanism was electrostatic interaction.[75] During the rapid removal of NO_3^- onto PANF, the decline in the binding energies of protonated amine (N3) and quaternary ammonium (N4) suggested that N3 and N4 played an important role in NO_3^- removal. An electrostatic attraction between the functional groups of the fiber and the NO_3^- ions
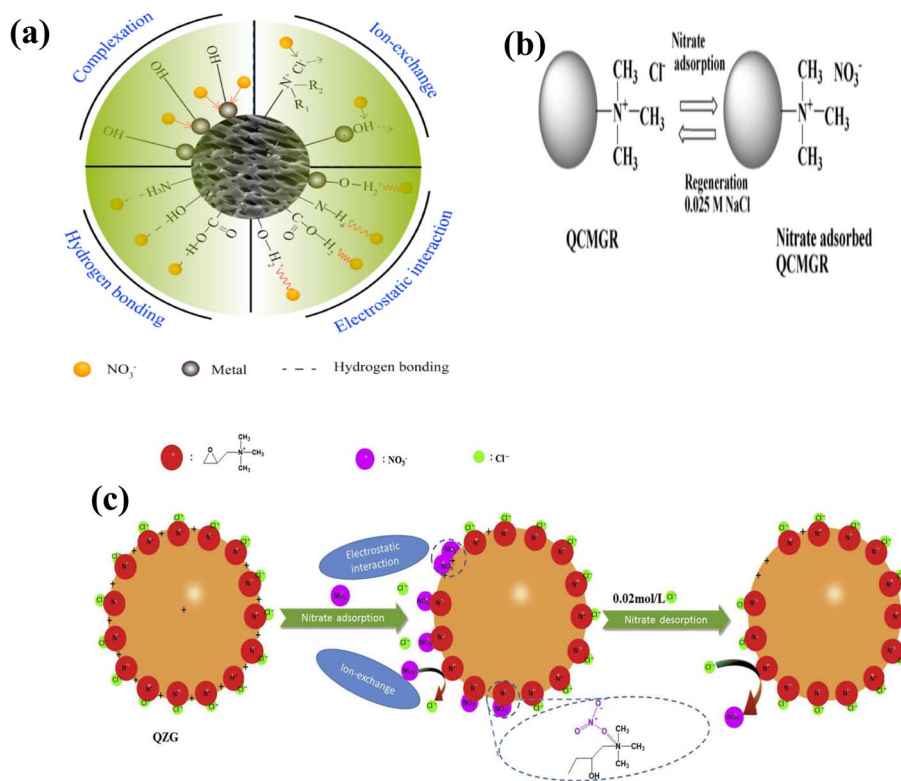
Fig. 9 (a) The possible adsorption possible adsorption sites and their corresponding adsorption mechanism {reproduced from ref. 40 with permission from Elsevier (License number–5874640053525)}, (b) Possible mechanism of anion adsorption/desorption by QCMGR {reproduced from ref. 93 with permission from Elsevier (License number–5874631111300)}, (c) the proposed mechanisms of nitrate ion adsorption by QZG {reproduced from ref. 99 with permission from Elsevier (License number–5874640184142)}.

were proposed as the mechanism for adsorption.[94] NO_3^- was effectively adsorbed on QCMGR by replacing Cl^- ions in the quaternary ammonium group *via* an ion exchange mechanism (Fig. 9b).[93] QZG-AER beads also effectively adsorbed the NO_3^- ions by replacing the Cl^- ion with a hydroxide ion through electrostatic adsorption.[99] The adsorption mechanism indicated that the primary cause of NO_3^- removal was electrostatic attraction between the positively charged quaternary sites and the negatively charged anions (Fig. 9c).[99] This was followed by an ion-exchange mechanism in which Cl^- ions were replaced in the medium. Also, the NO_3^- and hydroxyl groups found in the side chains possibly formed hydrogen bonding ($NO_3^- \cdots HO^-$).[90] The main adsorption mechanism for nitrate to adsorb onto Purolite A520E was coulombic forces.[123] Xu *et al.*[89] proposed that NO_3–N was adsorbed onto WR-AER through ion exchange, displacing chloride ions. Hence, the mechanism of NO_3–N sorption by WR-AER was represented by the following equation.

$$\dot{R}-N^+(CH_2CH_3)Cl^- + NO_3^- \leftrightarrow \dot{R}-N(CH_2CH_3)_3^+NO_3^- + Cl^-$$

7. Desorption and regeneration

When evaluating the practical application prospects of adsorbents, it is important to assess their reusability. For practical applications of industrial effluent treatment, it is important to

recover the adsorbed NO_3^- and reuse the AER. It is also necessary to analyze desorption and re-adsorption to gain an economic perspective on large-scale processes. In the literature, NaOH and HCl at different concentrations are commonly used as desorbing eluents. Table 5 summarizes the regeneration efficiency of the various AER. Especially from an industrial and environmental standpoint, the easy restoration of the resin and the ability to elute nitrate with sodium chloride (NaCl) solution make the water treatment method appealing.[88] In a subsequent study,[75] the NO_3^- adsorbed resin was brought in contact with various concentrations of NaCl. Using 0.6 M NaCl solution, *in situ* regeneration of the NDP-2 resin was performed, with 98% desorption efficiency. An almost identical result was obtained by using 0.3 M NaCl with a desorption equilibrium of 15 minutes, which corresponded to the faster adsorption rate.[94] In 0.2 N NaCl, the most efficient removal was found at the sixth cycle (>90%), which indicated NO_3^- elution was increased as the number of washing increased, making the resin more open to NO_3^- adsorption.[162] Another study[80] involved the use of 4 and 8 wt% NaCl solution to elute the NO_3^-- saturated resin, and 8 wt% salt solution achieved 99% desorption efficiency. In a recent study, Dharmapriya *et al.*[150] also used NaCl solution as the desorbing eluent at different concentrations to find out the reusability of hydrogel-based AER. During 15 cycles of regeneration, two hydrogel-based AER had adsorption capacities of 94.71% and 83.02% for NO_3^-, respectively. As a result of three

Table 5 Regeneration efficiency of various AER

Adsorbent	Solution	Regeneration efficiency (%)	Experiment mode	Reference
De-Acidite FFIP resin	0.1 M H_2SO_4	63	Batch	71
De-Acidite FFIP resin	5 M HCl	72	Batch	71
De-Acidite FFIP resin	0.1 M NaOH	93	Batch	71
Indion NSSR	NaCl	99.18	Column	95
NDP-2 resin	0.6 M NaCl	98	Column	75
Polyethylenimine-functionalized polyacrylonitrile anion exchange fiber	0.3 M NaCl	96	Column	94
WS anion exchange resins	1 M HCl	99.5	Batch	89
WS anion exchange resins	1 M HCl	98.4	Batch	119
WS anion exchange resins	1 M NaCl	96.1	Batch	119
Purolite A 520E resin	0.6 M NaCl	100	Column	120
Monolithic anion exchanger PolyHIPE media	1 M NaCl	99	Column	127
Strong basic anion exchange resin	0.2 N NaCl	90	Batch	162

cycles, Purolite A520E resin was able to remove 99.8%, 100%, and 100% of NO_3^- as shown in a recent study. It can be noted that, for cycles 1 through 3, 13.5 g, 14.25 g, and 10.8 g NaCl were required for 90% regeneration, respectively.[112] Using 1 M NaCl, there was hardly any difference in the remaining NO_3^- concentrations between the second and seventh cycles. This suggests that the modified Purolite A520E resin is practically reusable.[78] Regeneration of the D-890 ion exchange resin resulted in increased recovery with elevated NaCl concentrations from 3% to 6%, indicating improved effectiveness. The use of NaCl ensured relatively stable NO_3^- removal rates when concentrations exceed 6%, and a 95% recovery rate was consistently achieved. Zeng et al.[126] concluded that, considering economic and environmental factors, a 6% NaCl concentration is used for resin regeneration in practical engineering applications.

The HCl solution (1 M) was also used as an eluent and the desorption efficiencies for NO_3^- were found to be 99.5, 99.0, and 98.1% during three successive cycles for the use of AER made of agricultural by-products.[89] The weight loss of resin within the range of 12 to 18% was observed during desorption tests after the elution with HCl solution. It indicated the damage of cellulose structure in wheat straw (WS-AER) by HCl,

resulting in a decrease in the weight of the resin.[89] The monoliths were also regenerated with 1 N HCl, and the regeneration efficiency was 99% after the second cycle and 95% after the third cycle.[127]

To eliminate unadsorbed NO_3^- traces, De-Acidite FF-IP resin was washed several times with demineralized water. Next, it was eluted with various concentrations of eluents (acids and bases) to remove NO_3^- ions. The maximum desorption with 5 M HCl was 72%, whereas with 0.1 M H_2SO_4 only 63% desorption was observed. It was determined that 0.1 M NaOH, used as eluent, achieved the best NO_3^- ions recovery (93%) because OH- ions were exchanged with NO_3^- ions.[71]

In a study, NaCl and HCl were both used as eluents and both demonstrated excellent desorption capacity, indicating that NO_3^- ions were likely desorbed by ion exchange, which meant that the reverse of reactions with Cl^- in the NaCl or HCl solution displaced NO_3^- from the WS-AER. After four cycles of adsorption–desorption, only a slight loss in the adsorption capacities was observed, which confirmed that WS-AER can be used repeatedly to remove NO_3^- from aqueous solutions.[89] NDP-5 was regenerated and reused for ten cycles to assess its stability. It was found that adsorption capacity remained close to that of the first-time capacity after 10 adsorption–desorption

Table 6 Nitrate adsorption from bottled drinking water onto De-Acidite FF-IP resin {reproduced from ref. 71 with permission from Elsevier (License number-5874651371430)}

Commercially available bottled water[a]	Water source	NO_3^- level claimed in the label (mg L^{-1})	NO_3^- level before adsorption (mg L^{-1} ± SD)	NO_3^- level after adsorption (mg L^{-1})
Mawared	Well water	2.00	2.14 ± 0.02	Nd
Qassim	—	<10	4.21 ± 0.01	<LOQ
Safa	—	1.00	1.44 ± 0.03	nd
Hayat	Well water	6.00	6.49 ± 0.01	<LOQ
Nova	Well water	3.08	1.93 ± 0.02	Nd
Hana	Well water	3.00	3.00 ± 0.01	<LOQ
Hail	Well water	7.90	2.83 ± 0.02	<LOQ
Hada	—	5.00	4.82 ± 0.01	<LOQ
Fayha	Well water	4.00	3.74 ± 0.02	<LOQ
Berain	—	4.00	4.15 ± 0.01	<LOQ

[a] Sterilized by ozone; — not defined; SD = standard deviation ($n = 3$); nd = not detected. <LOQ = below limit of quantification; <LOD = below limit of detection.
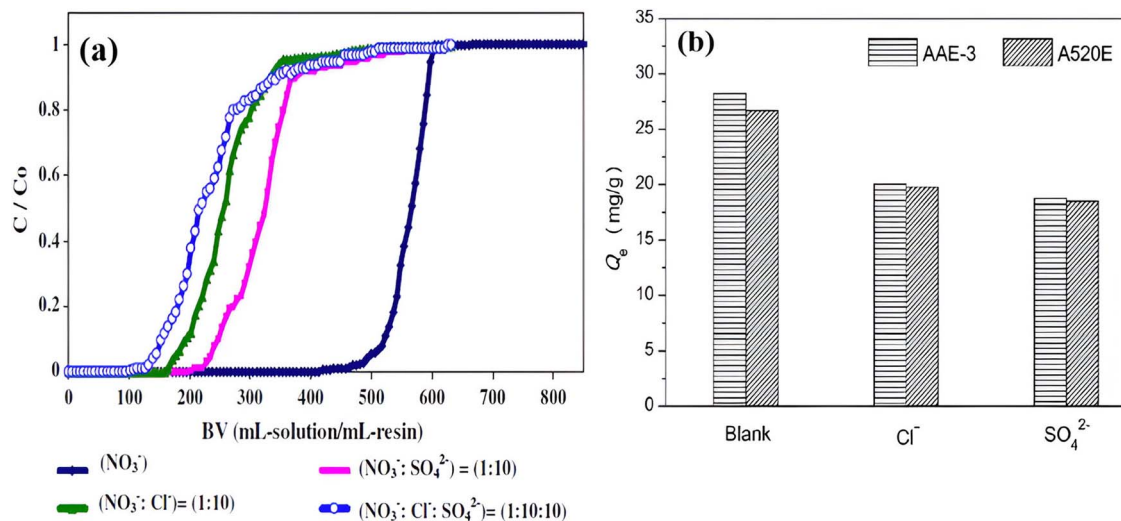
Fig. 10 (a) Effect of chloride and sulfate ions on nitrate removal by Purolite A 520E {reproduced from ref. 120 with permission from Elsevier (License number-5874670743228)}, (b) effect of competitive anions Cl$^-$ and SO$_4^{2-}$ on NO$_3^-$−N removal by two resins.[125]

cycles, and being steady with increasing cycle number. Based on these results, Song and Zhou[75] concluded that NDP-5 was a durable material that can be reused at least ten times in practical applications, which is an important factor.

8. Stability and practical utility

Generally, various coexisting ions in water strongly compete to occupy active sites. For this reason, determining the stability and selectivity of AER is essential for evaluating its practical application and adsorption ability. A practical test was conducted to evaluate the performance of the De-Acidite FF-IP resin in NO$_3^-$ removal from ten different samples of bottled water available on the market.[71] Upon measuring the NO$_3^-$ levels using the ultra-high performance liquid chromatography-MS method before and after adsorption (Table 6),[71] it was evident that the NO$_3^-$ levels in all bottled water samples were below 10 mg L^{-1} which after the adsorption process became nitrate-free in most of the samples. While in some samples, the NO$_3^-$ level was below the limit of detection, and the limit of quantitation. In a column test using Shiraz groundwater, Hekmatzadeh et al.[111] found that at the beginning of the experiment, nitrate and sulfate were adsorbed onto the IND-NSSR resin particles, while chloride was released due to the greater selectivity of the earlier anions. During water pass-through, sulfate ions adsorbed to the resin bed were released and replaced by nitrate ions. By this phenomenon, it is evident that the resin favored binding nitrate over sulfate with higher selectivity. Song et al.[75] discovered that competing anions affected NO$_3^-$ removal in the sequence of SO$_4^{2-}$ > Cl$^-$ > HCO$_3^-$. Notably, NDP-2 was effective at eliminating NO$_3^-$ from aqueous solutions containing different anions. There may be a reason for the higher selectivity of NDP-2 because its exchange sites have longer alkyl chains. It is expected that this technology will soon be widely used for purifying contaminated industrial water sources. In the process of NO$_3^-$ removal

from Purolite A520E resin using the column method, chloride and sulfate ions were present at concentrations ten times higher than that of nitrate. Both chloride and sulfate ions affected the breakthrough curves of nitrate; however, the presence of chloride had a greater impact than sulfate in shifting the breakthrough point (Fig. 10a).[120] A marginally higher NO$_3^-$ adsorption was observed for AEE-3 compared to A520E when an equal amount of anions was added. This can be attributed to the long alkyl chain on AEE-3, which enhanced the adsorption selectivity for NO$_3^-$ due to its lower hydration energy compared to Cl$^-$ or SO$_4^{2-}$ (Fig. 10b).[125] By determining the NO$_3^-$ removal capacity of PAN-PEI-5C under dissolved organic matter (DOM) conditions, the stability of poly-acrylonitrile fiber was assessed. Because DOM contains carboxylic (COOH) and phenolic (OH) groups, it can influence and occupy numerous active sites. The results indicated that PAN-PEI-5C exhibited remarkable stability in NO$_3^-$ uptake, even when reused in the presence of DOM.[94]

9. Conclusion and future perspectives

This review has demonstrated the utility of AER in water treatment. AER exhibits good selectivity and high capacity for the NO$_3^-$ adsorption process and can be effectively used as adsorbents. They exhibited good adsorption and desorption performance towards NO$_3^-$ ions. In batch mode, NO$_3^-$ removal by AER was found to depend on several factors such as pH, concentration, and time. Adsorption isotherm, kinetic, and thermodynamic studies were examined to determine how NO$_3^-$ adsorbed and its equilibrium concentration changed with temperature and concentration in contact with AER. As a result of this review, further research and commercial application of separation processes can be chosen that are most suitable for further investigation.
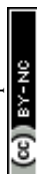
For a healthy environment and healthy population, removing toxic ions from aqueous systems is essential. As a result of previous studies, AER is effective in removing NO_3^- ions from water. The use of new resins, such as resins with alternative bio-based support matrixes, and disposable resins, and improving the economic process would be a very promising innovation. The design of new complex functional groups capable of chelating with nitrate in a fast and efficient manner at different pH levels is worth considering. Additionally, the combination of ion exchange and adsorption technology is possible. It is also possible to use resins with other water treatment technologies such as membrane separation. The future uses of inorganic sorbents such as magnetic nanoparticles and polymeric nanocomposite membranes are very promising. The design of resin-based adsorbents with a high capacity and lasting selectivity to remove NO_3^- is therefore of utmost importance. In recent years, various organic and inorganic nanoparticles have been used to manufacture nanocomposite membranes, including TiO_2, ZnO, Ag, graphene oxide, and SiO_2. In water treatment, polymer-inorganic ion exchange resins and hybrid nanocomposite membranes have significant potential. Molecular-scale particles can be effectively separated by membranes. There has been some recent progress in the creation of polymeric inorganic ion exchange resins which are capable of incorporating different types of nanoparticles to improve water purification and to separate different contaminants from the water.[163–166] For the removal of nitrate ions from simulated groundwater, nZVI was immobilized onto a Purolite A400 strongly base anion resin.[167] A Fe_3O_4/polyaniline nanocomposite was synthesized and tested for its superior ability to remove NO_3^- from urban wastewater.[168] The SE-1-AER was synthesized successfully to selectively remove NO_3^- from aqueous solutions based on asymmetric amines.[169] The sorption kinetics of SE-1-AER were faster than those of A 520E resin.[169] N-Alkylation of a weakly basic polyacrylic anion exchange resin D311 with 1-bromopropane resulted in the formation of a new AER i.e. AEE-3 for removing nitrate from aqueous solutions.[125] In the presence of DOM, AEE-3 resin exhibited better regeneration performance as opposed to the polystyrene-based nitrate resin Purolite A 520E.[125] In a recent study, bulk polymerization was used to produce an ion-imprinted polymer for adsorption of NO_3^- in polluted groundwater.[170] The removal of NO_3^- from aqueous solutions was achieved using polymer monoliths functionalized with PolyHIPE polymer.[127] The results of all these studies have shown that polymer-inorganic ion exchange resins can be used for NO_3^- adsorption and should therefore be considered for further research. To reduce energy costs, AER with high selectivity and reproducibility is required. Furthermore, further research is needed on the recovery of nitrate ions. There is a need to assess nitrate reduction methods simultaneously concerning other competing anions. It is still largely unknown how to safely treat and dispose of nitrate-adsorbed anion exchange resin. Therefore, future studies should focus on identifying environmentally friendly regeneration methods.

Data availability

No primary research results, software or code have been included and no new data were generated or analysed as part of this review.

Conflicts of interest

No potential conflict of interest was reported by the author(s).

Acknowledgements

References

1 World Health Organization, *Guidelines for Drinking-Water Quality: Fourth Edition Incorporating First Addendum*, World Health Organization, 4th edn + 1st add, 2017.

2 J. A. Simmons, *Environ. Toxicol. Chem.*, 2012, **31**, 1370–1374.

3 L. Juran and M. C. MacDonald, *J. Water Health*, 2014, **12**, 791–802.

4 X.-H. Zhang, *IERI Procedia*, 2014, **9**, 2–7.

5 H. Cui, X. Huang, Z. Yu, P. Chen and X. Cao, *RSC Adv.*, 2020, **10**, 20231–20244.

6 A. Cescon and J.-Q. Jiang, *Water*, 2020, **12**, 3377.

7 J. Gamiz, Y. Bolea, A. Grau, J. Gamiz, F. Luque and J. M. Vargas, in *IEEE 10th International Conference on Industrial Informatics*, IEEE, 2012, pp. 337–341.

8 M. K. Uddin, *Chem. Eng. J.*, 2017, **308**, 438–462.

9 M. K. Uddin and P. Rahaman, in *Inorganic Pollutants in Wastewater. Methods of Analysis, Removal and Treatment*, ed. Inamuddin, A. Mohammad and A. M. Asiri, Materials Research Forum LLC, 2017, pp. 149–186.

10 M. Simonič, *Membranes*, 2021, **11**, 976.

11 M. Mänttäri and M. Nyström, *Water Sci. Technol.*, 2007, **55**, 99–107.

12 C. Comninellis, A. Kapalka, S. Malato, S. A. Parsons, I. Poulios and D. Mantzavinos, *J. Chem. Technol. Biotechnol.*, 2008, **83**, 769–776.

13 M. Ikram, M. Rashid, A. Haider, S. Naz, J. Haider, A. Raza, M. T. Ansar, M. K. Uddin, N. M. Ali, S. S. Ahmed, M. Imran, S. Dilpazir, Q. Khan and M. Maqbool, *Sustainable Mater. Technol.*, 2021, **30**, e00343.

14 J. P. Ribeiro and M. I. Nunes, *Environ. Res.*, 2021, **197**, 110957.

15 M. Tariq, M. Muhammad, J. Khan, A. Raziq, M. K. Uddin, A. Niaz, S. S. Ahmed and A. Rahim, *J. Mol. Liq.*, 2020, **312**, 113399.

16 A. Ali, M. Sadia, M. Azeem, M. Z. Ahmad, M. Umar and Z. Ul Abbas, *Futuristic Biotechnol.*, 2023, 12–19.

17 P. Dydo and M. Turek, *Desalination*, 2013, **310**, 2–8.

18 I. Levchuk, J. J. Rueda Márquez and M. Sillanpää, *Chemosphere*, 2018, **192**, 90–104.
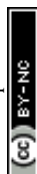
19 M. M. Hassan and C. M. Carr, *Chemosphere*, 2018, **209**, 201–219.

20 F. Dixit, R. Dutta, B. Barbeau, P. Berube and M. Mohseni, *Chemosphere*, 2021, **272**, 129777.

21 S. Wood, J. Henao and M. W. Rosegrant, *The Role of Nitrogen in Sustaining Food Production and Estimating Future Nitrogen Fertilizer Needs to Meet Food Demand*, 2004.

22 D. Dudley, *Environ. Prot. Agency*, 2011, **1049**, 2.

23 A. Bhatnagar and M. Sillanpää, *Chem. Eng. J.*, 2011, **168**, 493–504.

24 A. J. De Roos, M. H. Ward, C. F. Lynch and K. P. Cantor, *Epidemiology*, 2003, **14**, 640–649.

25 A. Mansouri and A. A. Lurie, *Am. J. Hematol.*, 1993, **42**, 7–12.

26 I. Ivek, T. Knotek, T. Ivičić, B. Rubinić, P. Bajlo and J. Hamžić, *Acta Clin. Croat.*, 2022, **61**, 93–98.

27 P. Sidhu, V. Mahajan, S. Verma, Ashuma and M. Gupta, *Toxicol. Int.*, 2014, **21**, 186.

28 J. A. Camargo, A. Alonso and A. Salamanca, *Chemosphere*, 2005, **58**, 1255–1267.

29 R. Ramya, *Haryana Vet.*, 2016, **55**, 237–238.

30 R. W. Herschy, *Encycl. Earth Sci. Ser.*, 2012, 876–883.

31 R. Picetti, M. Deeney, S. Pastorino, M. R. Miller, A. Shah, D. A. Leon, A. D. Dangour and R. Green, *Environ. Res.*, 2022, **210**, 112988.

32 E. Abascal, L. Gómez-Coma, I. Ortiz and A. Ortiz, *Sci. Total Environ.*, 2022, **810**, 152233.

33 A. Verma, A. Sharma, R. Kumar and P. Sharma, *Groundw. Sustain. Dev.*, 2023, **23**, 100978.

34 A. Mohseni-Bandpi, D. J. Elliott and M. A. Zazouli, *J. Environ. Health Sci. Eng.*, 2013, **11**, 1–11.

35 K. Velusamy, S. Periyasamy, P. S. Kumar, D.-V. N. Vo, J. Sindhu, D. Sneka and B. Subhashini, *Environ. Chem. Lett.*, 2021, **19**, 3165–3180.

36 F. Rezvani, M.-H. Sarrafzadeh, S. Ebrahimi and H.-M. Oh, *Environ. Sci. Pollut. Res.*, 2019, **26**, 1124–1141.

37 A. Gizaw, F. Zewge, A. Kumar, A. Mekonnen and M. Tesfaye, *Aqua Water Infrastruct. Ecosyst. Soc.*, 2021, **70**, 921–947.

38 N. Patel, A. L. Srivastav, A. Patel, A. Singh, S. K. Singh, V. K. Chaudhary, P. K. Singh and B. Bhunia, *Environ. Sci. Pollut. Res.*, 2022, **29**, 69137–69152.

39 P. Loganathan, S. Vigneswaran and J. Kandasamy, *J. Environ. Manage.*, 2013, **131**, 363–374.

40 Y. Liu, X. Zhang and J. Wang, *Chemosphere*, 2022, **291**, 132728.

41 M. Choudhary, M. Muduli and S. Ray, *Sustain. Water Resour. Manag.*, 2022, **8**, 113.

42 H. Liu, Z. Chen, Y. Guan and S. Xu, *Chemosphere*, 2018, **204**, 51–62.

43 M. Zhang, G. Song, D. L. Gelardi, L. Huang, E. Khan, O. Mašek, S. J. Parikh and Y. S. Ok, *Water Res.*, 2020, **186**, 116303.

44 X. Zou, C. Chen, C. Wang, Q. Zhang, Z. Yu, H. Wu, C. Zhuo and T. C. Zhang, *Sci. Total Environ.*, 2021, **800**, 149645.

45 B. Zhao, Z. Sun and Y. Liu, *Sci. Total Environ.*, 2022, **804**, 149981.

46 S. Yuan, Y. Xue, R. Ma, Q. Ma, Y. Chen and J. Fan, *Sci. Total Environ.*, 2023, **866**, 161444.

47 Z. Jia, T. Feng, M. Ma, Z. Li and L. Tang, *Surf. Interfaces*, 2024, **48**, 104294.

48 J. Wang and L. Chu, *Biotechnol. Adv.*, 2016, **34**, 1103–1112.

49 C. V. Lazaratou, D. V. Vayenas and D. Papoulis, *Appl. Clay Sci.*, 2020, **185**, 105377.

50 B. Bishayee, R. P. Chatterjee, B. Ruj, S. Chakrabortty and J. Nayak, *J. Environ. Manage.*, 2022, **303**, 114081.

51 S. Sevda, T. R. Sreekishnan, N. Pous, S. Puig and D. Pant, *Bioresour. Technol.*, 2018, **255**, 331–339.

52 F. de Dardel, *Ion Exchange Resin Structure*, **http://dardel.info/IX/resin_structure.html**.

53 H. A. Ezzeldin, A. Apblett and G. L. Foutch, *Int. J. Polym. Sci.*, 2010, **2010**, 684051.

54 ROHM & HASS, *Ion Exchange for Dummies: An introduction*, 2008, pp. 1–9.

55 N. A. S. Din, S. J. Lim, M. Y. Maskat, S. A. Mutalib and N. A. M. Zaini, *Bioresour. Bioprocess.*, 2021, **8**, 31.

56 H. Song, Z. Yao, C. Shuang and A. Li, *J. Ind. Eng. Chem.*, 2014, **20**, 2888–2894.

57 M. Alikhani and M. R. Moghbeli, *Chem. Eng. J.*, 2014, **239**, 93–104.

58 M. Abbasian, A. Ghaderi, H. Namazi and A. A. Entezami, *Polym.-Plast. Technol. Eng.*, 2011, **50**, 1606–1612.

59 A. Ghaderi, M. Abbasian, S. Rahmani, H. Namazi, H. Baharvand and A. A. Entezami, *Iran. Polym. J.*, 2006, **15**, 497–504.

60 M. Á. Vega-Hernández, G. S. Cano-Díaz, E. Vivaldo-Lima, A. Rosas-Aburto, M. G. Hernández-Luna, A. Martinez, J. Palacios-Alquisira, Y. Mohammadi and A. Penlidis, *Processes*, 2021, **9**, 375.

61 S. Uchida, *Encyclopedia of Polymeric Nanomaterials*, 2020, pp. 1–4.

62 M. A. Macchione, C. Biglione and M. Strumia, *Polymers*, 2018, **10**, 1–34.

63 A. Popat, J. Liu, G. Q. Lu and S. Z. Qiao, *J. Mater. Chem.*, 2012, **22**, 11173.

64 S. C. Hong, T. Pakula and K. Matyjaszewski, *Macromol. Chem. Phys.*, 2001, **202**, 3392–3402.

65 H. Paik, S. G. Gaynor and K. Matyjaszewski, *Macromol. Rapid Commun.*, 1998, **19**, 47–52.

66 L. Okrasa, T. Pakula, Y. Inoue and K. Matyjaszewski, *Colloid Polym. Sci.*, 2004, **282**, 844–853.

67 S. C. Hong, S. Jia, M. Teodorescu, T. Kowalewski, K. Matyjaszewski, A. C. Gottfried and M. Brookhart, *J. Polym. Sci., Part A: Polym. Chem.*, 2002, **40**, 2736–2749.

68 H. Shinoda, K. Matyjaszewski, L. Okrasa, M. Mierzwa and T. Pakula, *Macromolecules*, 2003, **36**, 4772–4778.

69 C. J. Hawker, D. Mecerreyes, E. Elce, J. Dao, J. L. Hedrick, I. Barakat, P. Dubois, R. Jérôme and W. Volksen, *Macromol. Chem. Phys.*, 1997, **198**, 155–166.

70 S. Tandorn, O.-A. Arqueropanyo, W. Naksata and P. Sooksamiti, *Int. J. Environ. Sci. Dev.*, 2017, **8**, 399–403.

71 M. Naushad, M. A. Khan, Z. A. ALOthman and M. R. Khan, *J. Ind. Eng. Chem.*, 2014, **20**, 3400–3407.

72 G. Liu, C. Han, M. Kong, W. H. M. Abdelraheem, M. N. Nadagouda and D. D. Dionysiou, *ACS ES&T Eng.*, 2022, **2**, 1454–1464.

73 D. Bekchanov, M. Mukhamediev, P. Lieberzeit, G. Babojonova and S. Botirov, *Polym. Adv. Technol.*, 2021, **32**, 3995–4004.

74 M. Davarpanah, A. Ahmadpour and T. Rohani Bastami, *J. Magn. Magn. Mater.*, 2015, **375**, 177–183.

75 H. Song, Y. Zhou, A. Li and S. Mueller, *Desalination*, 2012, **296**, 53–60.

76 Q. Li, X. Lu, C. Shuang, C. Qi, G. Wang, A. Li and H. Song, *Chemosphere*, 2019, **223**, 39–47.

77 W. Yang, J. Wang, X. Shi, H. Tang, X. Wang, S. Wang, W. Zhang and J. Lu, *Ind. Eng. Chem. Res.*, 2020, **59**, 5194–5201.

78 H. Zareie, F. Yazdani and B. Mokhtarani, *Mater. Chem. Phys.*, 2022, **285**, 126098.

79 Y. Tang, Q. Wen and Z. Chen, *Chem. Eng. J.*, 2023, **477**, 147137.

80 Y. Ren, Y. Ye, J. Zhu, K. Hu and Y. Wang, *Desalin. Water Treat.*, 2016, **57**, 17430–17439.

81 P. Cyganowski, Ł. Gruss, W. Skorulski, T. Kabat, P. Piszko, D. Jermakowicz-Bartkowiak, K. Pulikowski and M. Wiatkowski, *J. Water Process Eng.*, 2024, **59**, 104959.

82 Z. Shen, M. Fang, L. Tang, J. Shi and W. Wang, *Environ. Res.*, 2024, **241**, 117616.

83 G. Zhang, S. Li, C. Shuang, Y. Mu, A. Li and L. Tan, *Sci. Rep.*, 2020, **10**, 1–11.

84 A. Sowmya and S. Meenakshi, *Int. J. Biol. Macromol.*, 2014, **64**, 224–232.

85 S. Wiriyathamcharoen, S. Sarkar, P. Jiemvarangkul, T. T. Nguyen, W. Klysubun and S. Padungthon, *Chem. Eng. J.*, 2020, **381**, 122671.

86 D. S. Stefan, J. F. Van Staden, E. Vasile, O. R. Vasile and M. Dancila, *C. R. Chim.*, 2014, **17**, 738–745.

87 https://www.epa.gov/caddis-vol2/ph.

88 A. Keränen, T. Leiviskä, B.-Y. Gao, O. Hormi and J. Tanskanen, *Chem. Eng. Sci.*, 2013, **98**, 59–68.

89 X. Xu, B.-Y. Gao, Q.-Y. Yue, Q.-Q. Zhong and Q. Li, *Chem. Eng. J.*, 2011, **167**, 104–111.

90 H. T. Banu and S. Meenakshi, *Int. J. Biol. Macromol.*, 2017, **104**, 1517–1527.

91 C. Namasivayam and W. H. Höll, *J. Chem. Technol. Biotechnol.*, 2005, **80**, 164–168.

92 M. Chabani, A. Amrane and A. Bensmaili, *Desalination*, 2007, **206**, 560–567.

93 A. Sowmya and S. Meenakshi, *Int. J. Biol. Macromol.*, 2014, **64**, 224–232.

94 Y. Sun and W. Zheng, *Chemosphere*, 2020, **258**, 127373.

95 S. N. Milmile, J. V. Pande, S. Karmakar, A. Bansiwal, T. Chakrabarti and R. B. Biniwale, *Desalination*, 2011, **276**, 38–44.

96 N. Öztürk and T. E. Bektaş, *J. Hazard. Mater.*, 2004, **112**, 155–162.

97 X. Xu, B. Gao, Q. Yue, Q. Li and Y. Wang, *Chem. Eng. J.*, 2013, **234**, 397–405.

98 Y. Gu and Y. Sun, *Chem. Eng. J.*, 2024, **485**, 149650.

99 H. He, Y. Huang, M. Yan, Y. Xie and Y. Li, *Colloids Surf., A*, 2020, **584**, 123973.

100 T. T. Nguyen, V. A. K. Tran, L. B. Tran, P. T. Phan, M. T. Nguyen, L. G. Bach, S. Padungthon, C. K. Ta and N. H. Nguyen, *Chin. J. Chem. Eng.*, 2021, **32**, 378–384.

101 A. A. Hekmatzadeh, A. Karimi-Jashni, N. Talebbeydokhti and B. Kløve, *Desalination*, 2013, **326**, 125–134.

102 A. Norhayati, R. Muhammad and A. A. Kassim, *Mater. Today: Proc.*, 2019, **17**, 679–685.

103 U. Baig, M. K. Uddin and M. A. Gondal, *Colloids Surf., A*, 2020, **584**, 124031.

104 I. M. Alarifi, Y. O. Al-Ghamdi, R. Darwesh, M. O. Ansari and M. K. Uddin, *J. Mater. Res. Technol.*, 2021, **13**, 1169–1180.

105 M. K. Uddin and U. Baig, *J. Cleaner Prod.*, 2019, **211**, 1141–1153.

106 S. A. Aldahash, P. Higgins, S. Siddiqui and M. K. Uddin, *Sci. Rep.*, 2022, 1–19.

107 D. Z. Husein, M. K. Uddin, M. O. Ansari and S. S. Ahmed, *Environ. Sci. Pollut. Res.*, 2021, **28**, 28014–28023.

108 M. K. Uddin and A. Nasar, *Sci. Rep.*, 2020, **10**, 7983.

109 M. K. Uddin, F. Mashkoor, I. M. AlArifi and A. Nasar, *Mater. Res. Bull.*, 2021, **139**, 111279.

110 R. A. K. Rao and M. Kashifuddin, *Arabian J. Chem.*, 2016, **9**, S1233–S1241.

111 A. A. Hekmatzadeh, A. Karimi-Jashani, N. Talebbeydokhti and B. Kløve, *Desalination*, 2012, **284**, 22–31.

112 F. Labarca and R. Bórquez, *Sci. Total Environ.*, 2020, **723**, 137809.

113 I. Langmuir, *J. Am. Chem. Soc.*, 1916, **38**, 2221–2295.

114 H. M. F. Freundlich, *J. Phys. Chem.*, 1906, **57**, 385–470.

115 M. Temkin and V. Pyzhev, *Acta Physicochim. URSS*, 1940, **12**, 327–356.

116 S. Y. Elovich and O. G. Larionov, *Izv. Akad. Nauk SSSR, Otd. Khim. Nauk*, 1962, **2**, 209–216.

117 R. Sips, *J. Chem. Phys.*, 1948, **16**, 490–495.

118 J. Dron and A. Dodi, *J. Hazard. Mater.*, 2011, **190**, 300–307.

119 X. Xu, B.-Y. Gao, Q.-Y. Yue and Q.-Q. Zhong, *Bioresour. Technol.*, 2010, **101**, 8558–8564.

120 S. Samatya, N. Kabay, Ü. Yüksel, M. Arda and M. Yüksel, *React. Funct. Polym.*, 2006, **66**, 1206–1214.

121 M. Chabani, A. Amrane and A. Bensmaili, 2006, **125**, 111–117.

122 M. Das Gupta, P. Loganathan and S. Vigneswaran, *Sep. Sci. Technol.*, 2012, **47**, 1785–1792.

123 T. Nur, W. G. Shim, P. Loganathan, S. Vigneswaran and J. Kandasamy, *Int. J. Environ. Sci. Technol.*, 2015, **12**, 1311–1320.

124 F. Guesmi, I. Louati, C. Hannachi and B. Hamrouni, *Water Qual. Res. J.*, 2016, **51**, 106–116.

125 Y. Sun, W. Zheng, X. Ding and R. P. Singh, *Appl. Sci.*, 2019, **9**, 3077.

126 B. Zeng, B. Tao, Z. Pan, L. Shen, J. Zhang and H. Lin, *J. Environ. Manage.*, 2023, **347**, 119142.

127 N. Barlık, B. Keskinler, M. M. Kocakerim and G. Akay, *Desalin. Water Treat.*, 2016, **57**, 26440–26447.

128 T. Nur, M. A. H. Johir, P. Loganathan, S. Vigneswaran and J. Kandasamy, *Desalin. Water Treat.*, 2012, **47**, 50–58.

129 L. Divband Hafshejani, A. Hooshmand, A. A. Naseri, A. S. Mohammadi, F. Abbasi and A. Bhatnagar, *Ecol. Eng.*, 2016, **95**, 101–111.

130 X. Meng, L. Yao, W. Jiang, X. Jiang, C. Liu and L. Yang, *ACS Omega*, 2021, **6**, 1612–1622.

131 S. K. Ghadiri, S. Nasseri, R. Nabizadeh, M. Khoobi, S. Nazmara and A. H. Mahvi, *J. Mol. Liq.*, 2017, **242**, 1111–1117.

132 J. Chen, Y. Wei, H. Ji, P. Guo, D. Wan, B. Li and X. Sun, *Water Supply*, 2021, **21**, 4287–4300.

133 S. Najmi, M. S. Hatamipour, P. Sadeh, I. Najafipour and F. Mehranfar, *SN Appl. Sci.*, 2020, **2**, 773.

134 L. Wang, S. Liu, W. Xuan, S. Li and A. Wei, *Sustainability*, 2022, **14**, 7824.

135 Q. Hu, N. Chen, C. Feng, W. Hu and H. Liu, *RSC Adv.*, 2016, **6**, 61944–61954.

136 R. Khosravi, H. Eslami, A. Zarei, M. Heidari, A. N. Baghani, N. Safavi, A. Mokammel, M. Fazlzadeh and S. Adhami, *Desalin. Water Treat.*, 2018, **116**, 119–128.

137 D. Wan, H. Liu, R. Liu, J. Qu, S. Li and J. Zhang, *Chem. Eng. J.*, 2012, **195–196**, 241–247.

138 A. Ansari, E. T. Nadres, M. Đỗ and D. F. Rodrigues, *Process Saf. Environ. Prot.*, 2021, **150**, 365–372.

139 K. Hosni and E. Srasra, *Inorg. Mater.*, 2008, **44**, 742–749.

140 S. Hamoudi, R. Saad and K. Belkacemi, *Ind. Eng. Chem. Res.*, 2007, **46**, 8806–8812.

141 S. Chatterjee and S. H. Woo, *J. Hazard. Mater.*, 2009, **164**, 1012–1018.

142 A. Bhatnagar, M. Ji, Y. Choi, W. Jung, S. Lee, S. Kim, G. Lee, H. Suk, H. Kim, B. Min, S. Kim, B. Jeon and J. Kang, *Sep. Sci. Technol.*, 2008, **43**, 886–907.

143 Y. Zhang, X.-L. Song, S.-T. Huang, B.-Y. Geng, C.-H. Chang and I.-Y. Sung, *Desalin. Water Treat.*, 2014, **52**, 4935–4941.

144 W. Pan, R. Deng, Y. Cao, F. Xia, Q. Wu and L. Gu, *Desalin. Water Treat.*, 2021, **229**, 134–144.

145 S. K. M. Huno, J. Das, E. D. van Hullebusch, A. P. Annachhatre and E. R. Rene, *Syst. Microbiol. Biomanuf.*, 2023, **3**, 370–383.

146 N. Z. Pourbaghaei, M. Anbia and F. Rahimi, *J. Polym. Environ.*, 2022, **30**, 907–924.

147 Y. Shen, N. Chen, Z. Feng, C. Feng and Y. Deng, *Chemosphere*, 2022, **297**, 134107.

148 A. Gierak and I. Łazarska, *Adsorpt. Sci. Technol.*, 2017, **35**, 721–727.

149 M. Stjepanović, N. Velić and M. Habuda-Stanić, *Water*, 2022, **14**, 816.

150 T. N. Dharmapriya, H. Y. Shih and P. J. Huang, *Polymers*, 2022, **14**, 1442.

151 P. Ganesan, R. Kamaraj and S. Vasudevan, *J. Taiwan Inst. Chem. Eng.*, 2013, **44**, 808–814.

152 S. Hamoudi and K. Belkacemi, *Fuel*, 2013, **110**, 107–113.

153 E. Khoshkalam, A. Fotovat, A. Halajnia, H. Kazemian and H. Eshghi, *J. Mol. Liq.*, 2023, **375**, 121366.

154 Y. Wang, X. Song, Z. Xu, X. Cao, J. Song, W. Huang, X. Ge and H. Wang, *Water, Air, Soil Pollut.*, 2021, **232**, 198.

155 M. Jahangiri-rad, A. Jamshidi, M. Rafiee and R. Nabizadeh, *J. Environ. Health Sci. Eng.*, 2014, **12**, 90.

156 R. M. Kulkarni, B. D. Chalageri, A. Narula and A. Sachindran, *Nanotechnol. Environ. Eng.*, 2022, **7**, 405–413.

157 J. M. Angosto, J. M. Obón, M. J. Roca, M. Alacid and J. A. Fernández-López, *Agronomy*, 2023, **13**, 1325.

158 P. L. Homagai, R. Poudel, H. Paudyal, K. N. Ghimire and A. Bhattarai, *Environ. Sci. Pollut. Res.*, 2023, **30**, 54682–54693.

159 N. Aman, N. Ijaz, I. Fatima, M. U. Farid, H. Rashid, A. Ayub, D. A. Sabur, I. T. Ibrahim, H. M. Abd El-Lateef, I. Rafique, Y. Mehmood and R. M. K. Mohamed, *Geol. Ecol. Landscapes*, 2023, 1–12.

160 H. Zhou, Y. Tan, W. Gao, Y. Zhang and Y. Yang, *Sci. Rep.*, 2020, **10**, 16126.

161 M. Fizir, A. Richa, S. Touil, Y. Benmokadem, K. Boubekeur, B. Hallal, H. Drici and L. Wei, *Environ. Prog. Sustainable Energy*, 2023, **42**, 13995.

162 R. R. Yaragal and S. Mutnuri, *Int. J. Environ. Sci. Technol.*, 2023, **20**, 739–754.

163 Z. Deng, Z. Fang, A. Liu, N. Xu and X. Zhang, *Sci. Total Environ.*, 2021, **777**, 146103.

164 T. V. Maltseva, E. O. Kolomiets, Y. S. Dzyazko and S. Scherbakov, *Appl. Nanosci.*, 2019, **9**, 997–1004.

165 M. Li, B. Zhang, S. Zou, Q. Liu and M. Yang, *J. Hazard. Mater.*, 2020, **384**, 121386.

166 U. Hani, *Alexandria Eng. J.*, 2023, **72**, 307–321.

167 O. D. Orbuleț, A. M. Dăncilă, S. Căprărescu, C. Modrogan and V. Purcar, *Polymers*, 2022, **15**, 61.

168 R. Katal, S. Pourkarimi, E. Bahmani, H. A. Dehkordi, M. A. Ghayyem and H. Esfandian, *J. Vinyl Addit. Technol.*, 2013, **19**, 147–156.

169 Y. Sun, W. Zheng, X. Ding and R. P. Singh, *Adsorpt. Sci. Technol.*, 2020, **38**, 271–285.

170 W. Li, Y. Li, P. Cai, M. Zhang, T. Xia, X. Liang, W. Xiao and J. Dong, *J. Water Process Eng.*, 2023, **51**, 103375.